PREPARATION OF BTS-BCT THIN FILMS BY CHEMICAL SOLUTION DEPOSITION AND THEIR CHARACTERIZATION

A THESIS SUBMITTED TO
THE GRADUATE SCHOOL OF NATURAL AND APPLIED SCIENCES
OF
MIDDLE EAST TECHNICAL UNIVERSITY

BY

BERK AKBAY

IN PARTIAL FULFILLMENT OF THE REQUIREMENTS
FOR
THE DEGREE OF MASTER OF SCIENCE
IN
METALLURGICAL AND MATERIALS ENGINEERING

FEBRUARY 2015

Approval of the thesis:

PREPARATION OF BTS-BCT THIN FILMS BY CHEMICAL SOLUTION DEPOSITION AND THEIR CHARACTERIZATION

submitted by **BERK AKBAY** in partial fulfillment of the requirements for the degree of **Master of Science in Metallurgical and Materials Engineering Department, Middle East Technical University** by,

Prof. Dr. Gülbin Dural Ünver
Dean, Graduate School of **Natural and Applied Sciences** _____

Prof. Dr. Cemil Hakan Gür
Head of Department, **Metallurgical and Materials Engineering** _____

Prof. Dr. Ahmet Macit Özenbaş,
Supervisor, **Metallurgical and Materials Engineering Dept.,METU** _____

Examining Committee Members:

Prof. Dr. Cevdet Kaynak
Metallurgical and Materials Engineering Dept., METU _____

Prof. Dr. Ahmet Macit Özenbaş
Metallurgical and Materials Engineering Dept., METU _____

Prof. Dr. A. Caner Durucan
Metallurgical and Materials Engineering Dept., METU _____

Assoc. Prof. Dr. Burcu Akata Kurç
Micro and Nanotechnology Dept., METU _____

Assist. Prof. Dr. M. Bilge İmer
Metallurgical and Materials Engineering Dept., METU _____

Date: 05.02.2014

I hereby declare that all information in this document has been obtained and presented in accordance with academic rules and ethical conduct. I also declare that, as required by these rules and conduct, I have fully cited and referenced all material and results that are not original to this work.

Name, Last Name: Berk AKBAY

Signature:

ABSTRACT

PREPARATION OF BTS-BCT THIN FILMS BY CHEMICAL SOLUTION DEPOSITION AND THEIR CHARACTERIZATION

Akbay, Berk

M.S., Department of Metallurgical and Materials Engineering
Supervisor: Prof. Dr. Ahmet Macit Özenbaş

February 2015, 93 pages

In the presented thesis, lead-free $Ba(Ti_{0.88}Sn_{0.12})O_3$-$0.3(Ba_{0.7}Ca_{0.3})TiO_3$ (BTS-BCT) thin films were deposited on (111)-Pt/TiO_2/SiO_2/(100)-Si substrates using chemical solution deposition method and then the effect of process parameters were investigated to obtain optimum parameters of these lead-free thin films. The phase was selected near to the morphotropic phase boundary (MPB) to increase the number of polarization directions where rhombohedral and tetragonal phases exist together.

In this study, the effect of sintering temperatures on microstructure, dielectric and ferroelectric properties were studied systematically. Among the various high-quality BTS-BCT thin films with uniform thickness, the optimum dielectric and ferroelectric responses were observed for films sintered at 850^{o}C for 1 h sintering time. The thickness was kept constant for all measurements as 500 nm (thirteen layered films).

BTS-BCT thin films sintered at 850^{o}C for 1 h exhibited effective remnant polarization and coercive field values of 4.11 μC/cm^2 and 57.8 kV/cm, together with a dielectric constant and low loss tangent of 113.4 and 5.46 %, respectively, at a frequency of 600 kHz due to perovskite phase formed by crystallization, minimum surface porosity and larger grains obtained at this temperature.

Keywords: Chemical Solution Deposition, Lead-Free Thin Films, BTS-BCT, Ferroelectric Properties, Dielectric Properties.

ÖZ

BTS-BCT İNCE FİLMLERİN KİMYASAL ÇÖZELTİDEN BİRİKTİRME YÖNTEMİYLE HAZIRLANIŞI VE KARAKTERİZASYONU

Akbay, Berk
Yüksek Lisans, Metalurji ve Malzeme Mühendisliği Bölümü
Tez Yöneticisi: Prof. Dr. Ahmet Macit Özenbaş

Şubat 2015, 93 sayfa

Yapılan tez çalışması kurşunsuz baryum titanat esaslı $Ba(Ti_{0.88}Sn_{0.12})O_3$-$0.3(Ba_{0.7}Ca_{0.3})TiO_3$ (BTS-BCT) ince filmlerin (111)-Pt/TiO_2/SiO_2/(100)-Si altlıkları üzerine kimyasal çözelti biriktirme yöntemiyle büyütülmeleri ve denenen süreç parametrelerinin en uygun film üretimi üzerine etkisinin araştırılmasıdır. İdeal film üretiminin gerçekleştirilmesi amacıyla kompozisyon rombohedral-tetragonal fazların bir arada gözlemlendiği morfotropik faz sınırına yakın seçilmiştir.

Bu tez çalışmasında, üretilen ince filmlerin ferroelektrik ve dielektrik özelliklerinin birbirleri ile olan ilişkisi ve sinterleme sıcaklıklarının ince filmlerin mikroyapı ve morfolojisi üzerine olan etkisi sistematik bir şekilde incelenmiştir. Uygulanan değişik sinterleme sıcaklıkları içerisinde, en uygun ferroelektrik ve dielektrik özellikler 850°C'de 1 saat süreyle sinterlenen filmlerde gözlemlenmiştir. Bütün çalışma boyunca, film kalınlığı 500 nm (on üç katmanlı film) olarak sabitlenmiştir.

En iyi ferroelektrik özellikler 850°C'de 1 saat süreyle sinterlenen filmlerde elde edilmiş olup, kalıcı polarizasyon 4.11 $\mu C/cm^2$ ve koersiv alan 57.8 kV/cm olarak ölçülmüştür. Bu filmlerde dielektrik sabiti ve dielektrik kaybının 600 kHz frekansta elde edilen değerleri de sırasıyla 113.4 ve % 5.46 olarak kaydedilmiştir. Bunun nedeninin 850°C'de sinterlenen filmlerde kristalizasyon neticesinde oluşan perovskit

fazı, düşük yüzey porozitesi ve iri tanecik büyüklüğünden kaynaklandığı düşünülmektedir.

Anahtar Sözcükler: Kimyasal Çözelti Biriktirme, Kurşunsuz İnce Filmler, BTS-BCT, Ferroelectrik Özellikler, Dielektrik Özellikler.

To science as a candle in the dark…

ACKNOWLEDGEMENTS

More than anyone, I would like to express my sincere gratitude to my supervisor Prof. Dr. Macit Özenbaş for his endless support, guidance, patience, supervision and encouragement during entire study.

I thank to Surface Science Research Laboratory present and former staff Murat Güneş, Kerem Çağatay İçli, Halil İbrahim Yavuz, Barış Çeltikçi, Bahadır Can Kocaoğlu, Utku Er for their support in any issue related to study and sincere friendship.

I also thank to my manager Fatih Alim and my colleagues in Turkish Atomic Energy Authority, who supported me at work and encouraged me to go on thesis study.

I would like to express my gratefulness to my beloved family for giving me a chance to do science and my sincere happiness for their endless love and support for all of my life. I believe that I have not frustrated their trust in me.

Starting from my teachers in primary school to my instructors in Metallurgical and Materials Engineering Department of METU, I thank to all educators for their altruistic efforts especially.

Lastly, I would like to express my final gratitude to “legendary scientist” Carl Sagan, who spent all of his life to make the people of the world understand the wonders of the cosmos and learn, use and love the science.

TABLE OF CONTENTS

LIST OF TABLES

TABLES

LIST OF FIGURES

FIGURES

CHAPTER 1

INTRODUCTION

For more than fifty years, the lead based compositions have dominated electronics market due to their capability in electrical applications from non-volatile memories to capacitors, medical ultrasound actuators, micro electromechanical systems (MEMs) [1-3]. Among the applications of lead based compositions as thin films and bulk materials, piezoelectric thin films have been widely used because of having many advantages such as high economical markets such as non-volatile memories and MEMs, design flexibility with lithographic processes to fabricate and low operating voltages are some of the advantages.

Particularly, among lead based compositions the PZT phase (lead zirconate titanate) is widely used due to having superior electrical properties such as ferroelectricity and piezoelectricity. Compositionally, in its phase diagram, perovskite PZT ceramics exist close to morphotropic phase boundary (MPB) which separates perovskite ferroelectric phases. Compositions at MPB have extremely high dielectric, ferroelectric, piezoelectric properties which are provided by enhanced polarizability due to coupling between to equivalent energy states of ferroelectric tetragonal and ferroelectric rhombohedral phases, allowing minimum domain switching [4]. When compared with other MPB phases, the main factor that made the widely usage of PZT due to large piezoelectric response is provided by the $6s^2$ lone pair of lead ion which induce prominent lattice distortions in cubic phase which provides strong coupling between the electronic and structural degrees of freedom [5].

Many coating techniques are present for deposition of PZT thin films such as ion beam sputtering (IBS), magnetron sputtering (PVD), chemical vapor deposition (CVD), pulsed laser deposition (PLD) and chemical solution deposition (CSD) [6].

An aspect of chemical solution deposition, sol-gel processing for PZT thin film production has given prominence due to four unique advantages. Firstly, the chemical composition stoichiometry can be set easily which is highly important for complex oxides due to the fact that the physical properties of them likely depend on the chemical composition accuracy. Secondly, sol-gel production for thin films is cheap due to the fact that precursors can be used completely. Another advantage of sol-gel method is its suitability for mass production and compatibility with different device production methods. Finally, the microstructures can be patterned directly and conventional etching can be eliminated. All of the factors mentioned have made sol-gel processing more advantageous to produce PZT thin films [7]. As a result chemical solution deposition technique was chosen to fabricate lead-free thin films.

In spite of the fact that PZT materials have superior properties, the lead based compositions are hazardous for health and environment because of the toxic effect due to lead content. Therefore, to use lead based materials is prohibited step by step in European Union and Turkey for civil applications [8-10]. Hence, alternative phases to PZT material have been studied intensively. Among lead free alternatives, in general three main families; alkaline niobates, bismuth sodium titanates and barium titanates including the modified compositions of these material families outshine [11].

Alkaline niobates have been studied extensively since ferroelectricity in potassium niobate, $KNbO_3$ (KN) was discovered in the beginning of half of 20^{th} century. Compositionally modified KN-based compositions possess higher piezoelectric properties and phase transition temperatures. Potassium sodium niobates (KNN) have been studied widely but the main difficulty for potassium sodium niobates is to obtain fully dense ceramic body [12].

Since 1960s, bismuth sodium titanate (BNT) has also been studied due to its ferroelectric properties. Nevertheless pure bismuth sodium titanate phase has problems caused by large coercive field and high conductivity that results in difficult poling which cause weak polarization. For this reason different methods are studied for this lead free system [13].

The last lead-free family is barium titanates. This perovskite phase has been widely combined with KNN and BNT phases in order to obtain dense microstructures. Even so, very high piezoelectric properties have been published in the phases based on barium titanates which are succeeded by addition of tin, calcium and zirconium [14-18]. Similar to PZT, the high piezoelectric effect is provided by having tricritical point on phase diagram of those compositions which are tin, calcium, zirconium added barium titanate based compositions. Theoretically, if the composition of the material is exactly at tricritical point, there is no energy barrier for polarization rotation between tetragonal and rhombohedral phases [19]. Lead-free families other than barium titanate based compositions, KNN and BNT based compositions do not possess tricritical point thus results in energy barrier for polarization rotation between tetragonal and rhombohedral phases that leads to an important decrease in piezoelectric properties[20].

Electrical properties of barium titanate based $Ba(Ti_{0.88}Sn_{0.12})O_3$-$0.3(Ba_{0.7}Ca_{0.3})TiO_3$ in bulk forms, have been studied in a few studies recently even though the results are encouraging for lead-free alternative material [19]. On the other hand, the thin film form of this phase has not been studied. For this reason, this study has the aim to fabricate this recently studied phase of $Ba(Ti_{0.88}Sn_{0.12})O_3$-$0.3(Ba_{0.7}Ca_{0.3})TiO_3$ in thin film form. The ferroelectric and dielectric properties have been studied systematically. Crack free thin films having 500 nm film thickness have been fabricated by sol-gel method. In order to have a columnar growth of the the films which provides enhanced ferroelectric properties, the molarity of the solvent was kept relatively low, 0.4M. By thermal analysis of powders which were deposited by precipitation of the solvent, thermal properties were determined that is related with phase analysis, dielectric and ferroelectric properties. In this manner, according to electrical properties, optimum production conditions thin films with $Ba(Ti_{0.88}Sn_{0.12})O_3$-$0.3(Ba_{0.7}Ca_{0.3})TiO_3$ composition have been determined.

This thesis consists of five chapters. The next chapter is separated for literature survey. Alternatives to lead-based piezoelectric thin films, the main lead-free families proper for thin film applications are explained and their electrical properties

are compared. Theoretical approaches for dielectric, ferroelectric and piezoelectric properties were explained. The third chapter gives the details of experimental procedure. In chapter four, the results of the experiments were given and discussed. The discussions consist of theoretical approaches and analyses. Lastly, the outcome of the study was defined and further suggestions were proposed.

CHAPTER 2

LITERATURE SURVEY

2.1. Dielectric Properties of Materials

2.1.1. Dielectric Properties

In material science fundamental book of Callister, a dielectric material is defined as electrically insulating (nonmetallic) material which has an electric dipole structure which is separation of opposite charged particles on atomic or molecular level [21].

Simply, a capacitor is a device which stores electric charge. If voltage is applied, in a capacitor there are two conductors with equal amount but opposite charges and the total net charge on the capacitor is zero. If there is no applied voltage, then on either conductor no charge exists.

In a capacitor, the amount of charge Q (Coulomb) stored is linearly proportional with ΔV (Volt), the electrical potential difference between the plates,

$$Q = C\Delta V \qquad \text{Eq. [2.1]}$$

where C is capacitance. C is proportionality constant and SI unit of C is farad (F). A simple way to demonstrate a capacitor consisting two conducting parallel plates to each other with area A, having distance d between each other separating two equal amount but oppositional positive +Q, negative -Q charges can be shown in Figure 2.1

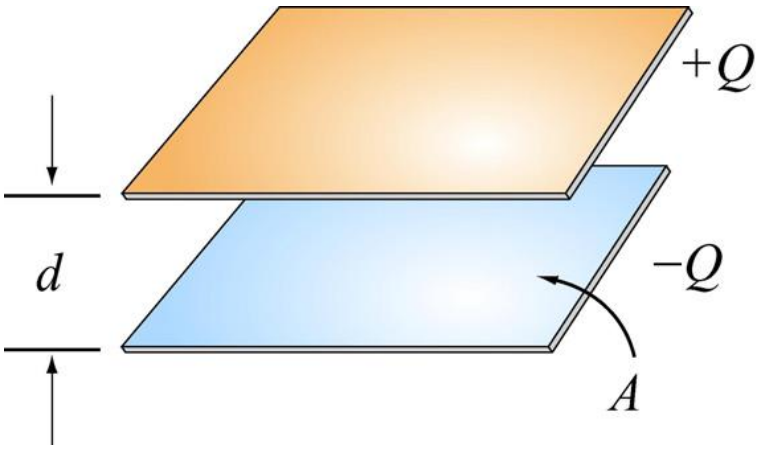

Figure 2.1 A parallel plate capacitor [22]

In the situation when vacuum exists between the plates;

$$c_o = \frac{\epsilon_0 \times A}{d} \qquad \text{Eq. [2.2]}$$

where ϵ_o is permittivity of vacuum, 8.85x10^{-12} F/m, d represents distance between the plates separating conductors and A is area of the plates. So the capacitance C increases linearly with area A, while decreases inversely proportional with distance d for a specific ΔV.

When a dielectric material is put between plates under vacuum conditions,

$$C = \frac{\epsilon \times A}{d} \qquad \text{Eq. [2.3]}$$

where ϵ respresents the permittivity of dielectric material, d for thickness of the dielectric material and A for area of plates.

Dielectric constant is the relative permittivity ϵ_r, of a dielectric material. It is permittivity ratio of the dielectric medium to permittivity of vacuum.

$$\epsilon_r = \frac{\epsilon}{\epsilon_o} \qquad \text{Eq. [2.4]}$$

Consequently,

$$C = \frac{\epsilon_r \times \epsilon_o \times A}{d} \qquad \text{Eq. [2.5]}$$

where ϵ_r represents dielectric constant of the material while ϵ_o represents the permittivity of vacuum, 8.85×10^{-12} F/m, d for the thickness of the material, A for contact area.

Generally capacitors are used in alternating current. Some part of the excitation energy is taken in and converted to heat energy in these voltages. This transferring is called tangent loss (tan δ) or dielectric loss. The charge on a dielectric material exhibit two parts, one of them is real (in phase) and the other one is imaginary (out of phase) which is due to dielectric absorption or resistive leakage. The dielectric loss is identified by the ratio of out of phase part to in phase part. The dielectric loss shown as D represents the dissipation factor.

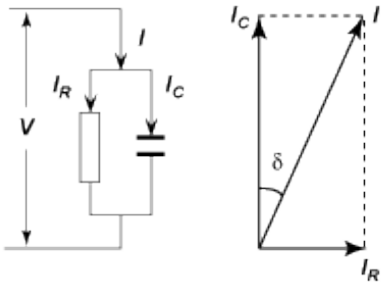

(a) (b)

Figure 2.2 Equilavent circuit for dielectric loss (a) charging and loss current (b) dielectric loss in vectorial illustration [23]

As vectorial, the total current is composed of two parts, the charging current and the loss current. δ represents angle between the vector of total current and charging current. The tangent loss is the tangent of δ.

$$\tan \delta = (\text{loss current})/(\text{charging current}) = \frac{\epsilon''}{\epsilon'} \qquad \text{Eq. [2.6]}$$

where ϵ'' is out of phase part and ϵ' is in phase part of the permittivity.

2.1.2. Polarization

Maybe the best approach to explain capacitance phenomenon is to describe polarization process of dielectric materials. In Figure 2.3 a simple electric dipole is illustrated.

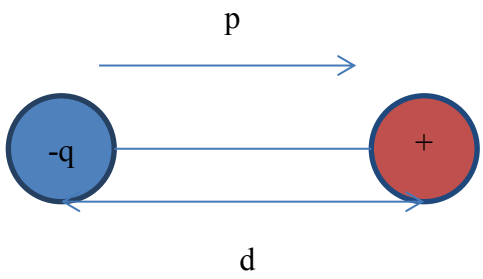

Figure 2.3 A simple electric dipole originated by positive and negative charges with charge magnitude q, distance d and polarization vector p

An electric dipole moment ***p***,:

$$\boldsymbol{p} = q \times d \qquad \text{Eq. [2.7]}$$

where q represents the charge magnitude of individual dipoles and d represents the distance. Figure 2.3 also shows a dipole moment, which is a vector starting from negative to positive charge. When electric field $\mathscr{E}$ is applied, a force will keep on the electric dipole to have the same polarization direction with the direction of applied field; which is shown in Figure 2.4. This change of dipole arrangement in a line is polarization.

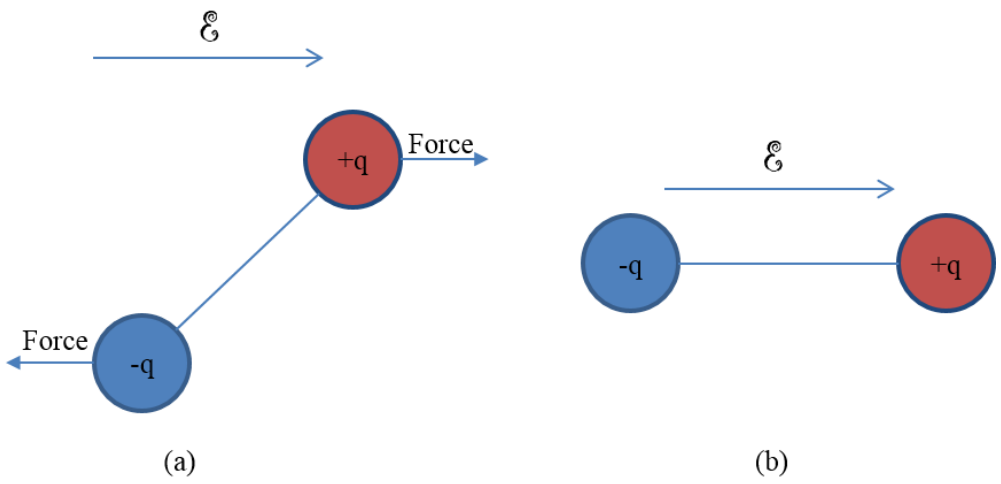

Figure 2.4 (a) Imposed forces on a dipole by an electric field. (b) Final arrangement of dipoles in a line due to the field

D, called as surface charge density, which can be also defined as the charge quantity per unit area of the capacitor plate (C/m^2) is proportional to the electric field applied. Under vacuum,

$$D_0 = \epsilon_o \times \mathscr{E} \qquad \text{Eq. [2.8]}$$

where the constant of proportionality being permittivity of vacuum ϵ_o. For dielectric capacitors,

$$D = \epsilon \times \mathscr{E} \qquad \text{Eq. [2.9]}$$

where ϵ is permittivity of the dielectric medium and D is also called dielectric displacement.

Electronic, ionic and orientation polarizations are three sources for total polarization. Firstly, the electronic polarization $\boldsymbol{P_e}$, is provided by the movement of the center of negatively charged electron cloud by electric field relative to the location of positively charged nucleus of an atom. This type of polarization exists only when electric field is applied. Another type, ionic polarization $\boldsymbol{P_i}$, takes place only ionic materials. These type of materials possess cations and anions which are slightly

displaced from equilibrium positions when electric field is applied and by this way increase net dipole moment. Lastly, orientation polarization $\boldsymbol{P_o}$ occurs only in materials which exhibit permanent dipole moments. Orientation polarization is provided by rotations of the permanent dipole moments into the direction of the applied field. The dielectrics possess one or more than one of three types of polarizations [24].

The total polarization $\boldsymbol{P}$ can be defined as,

$$\boldsymbol{P} = \boldsymbol{P_e} + \boldsymbol{P_i} + \boldsymbol{P_o} \qquad \text{Eq. [2.10]}$$

2.2.Ferroelectric Properties of Materials

2.2.1. Ferroelectric Phenomena

Ferroelectricity is the spontaneous alignment of dipoles as a result of their mutual interactions. At lower temperatures, the electric dipoles in a ferroelectric material create a local field that is stronger than the thermal energy required for randomization and spontaneous polarization results. Without external applied forces, the dipoles align in regions or domains.

These compounds are typically cubic (centrosymmetric) and therefore paraelectric at high temperatures. As the material is cooled, a change to a ferroelectric phase occurs at the Curie temperature, T_C, and spontaneous polarization results. The perovskite ferroelectric phase is generally tetragonal or rhombohedral. Most of the perovskite compounds readily form solid solutions with one another, allowing substantial substitution to achieve optimal performance (in this thesis, barium stannate titanate and barium calcium titanate solid solution). When a ferroelectric is cooled through its Curie region, the cubic lattice deforms to a polar phase. The polarization orients into regions, or domains, so as to minimize intergranular stresses. The dipoles of adjacent domains align along crystallographic axes [24,25].

Figure 2.5 shows the structure of a perovskite ABO_3, in the centrosymmetric-cubic

and ferroelectric-tetragonal phases. ABO_3 is the general expression for perovskite, A atoms (Ba^{+2} and Ca^{+2} in this study) symbolize cations that locate at the unit cell corners, and B atom (Sn^{+4} or Ti^{+4} in this study) symbolize other cation with higher valence electron which has position at the perovskite crystal center and O^{-2} is oxygen anions that surround the cations of B type in octahedra. At temperatures higher than T_C, the crystal has cubic structure and center atom is in centro-symmetric position. Thus no dipole moment is obtained. Below T_C cubic phase converts to tetragonal perovskite phase. This change occurs by the movement of B type cations in the O_6 octahedra due to the internal stresses. These internal stresses are the main factor for non-centrosymmetry that leads to spontaneous polarization, hence enable existence of ferroelectric property.

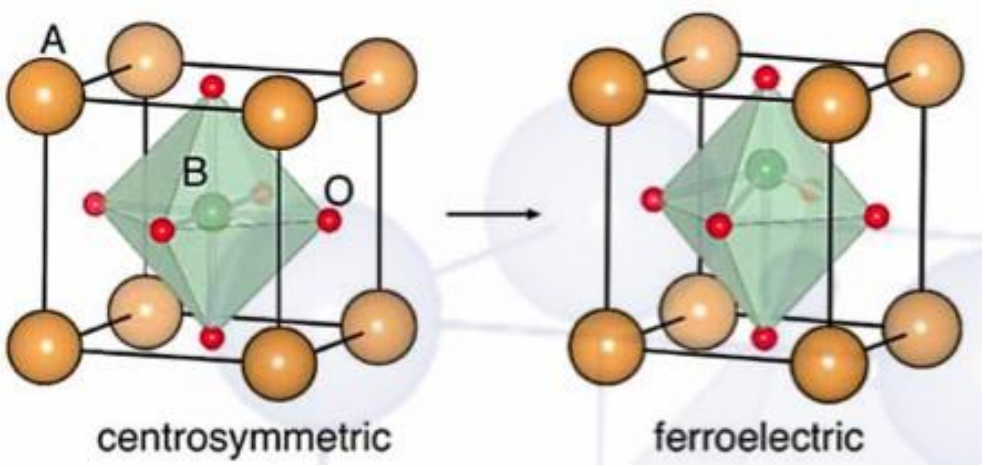

Figure 2.5 (a) The structure of a perovskite, ABO_3, in the centrosymmetric-cubic (left) and the ferroelectric-tetragonal phase (right) [26]

The main property of ferroelectrics can be settled as polarization reversal (or switching) when an electric field is applied. The ferroelectric hysteresis is an import tool to determine ferroelectric properties can be seen in Figure 2.6. Firstly, when electric field is applied, at between AC electric field, the polarization AB promotes linearly. This is due to the fact that AC electric field is not sufficient to provide polarization reversal. However when the electric field is strengthened the domains will begin to orient compatible with the field orientation. This will result in fast and nonlinear promotion in polarization density, BC. The domains are completely align

with the electric field and reach the saturation at D. The line between CD can be extrapolated in order to obtain the spontaneous polarization, P_S. When the field magnitude decreases some amount of the domains will reverse and if no electric field is applied at point E, the polarization is called remnant polarization, P_R. If the field begins to increase in negative direction, the curve reaches a point where there is no net polarization; F is coercive field which is shown as E_C [27].

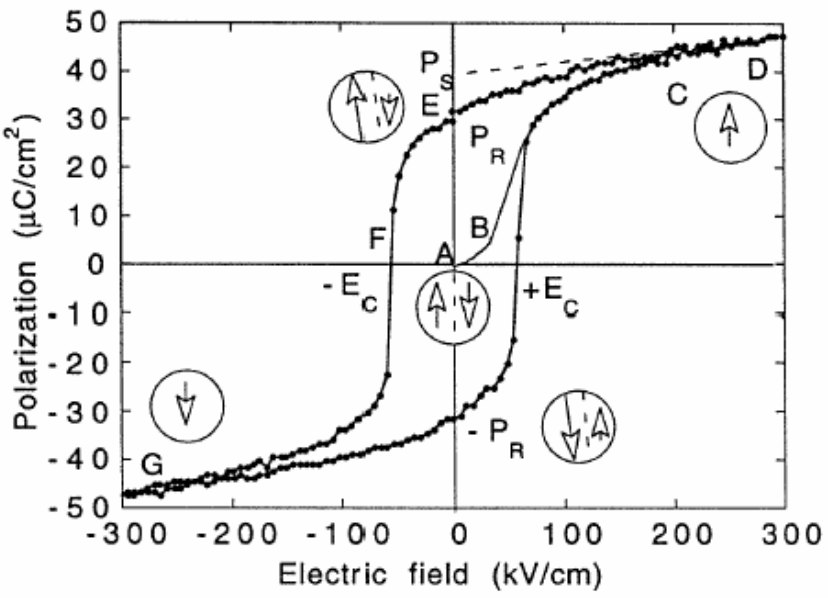

Figure 2.6 Ferroelectric Polarization versus Electric Field hysteresis loop. The arrows in the circles show the polarization direction of domains [27]

When electric field is applied the material is polarized that decreases its energy via the dipole moments having parallel direction with the electric field are decreased in energy. In contrast, the moments having perpendicular direction with the electric field have higher energy, on the top of it anti-parallel moments have highest energy. If a material is completely polarized, the domains of that material utterly have arrangement in a line. When electric field with reverse potential is applied, then nucleation of new domains having polarization with a reverse direction begins heterogeneously. The nucleation needs some time but it is fast. When these nuclei achieve to exhibit the critical size, they get larger from interior toward the exterior and, thus needle-like structure form. Once these needle-like structures extend the

edge of film, they start to get widened. As shown in Figure 2.6, the removal of the electric field leaves some polarization behind, the remnant polarization. These domains get larger fast that result in an important change of polarization with a small change in electric field. However formation of completely switched material requires large electric field applied. This requirement have been related both with defects in the crystal structure and stray field energy. These three sections mentioned about the minor hysteresis curve is shown in Figure 2.7.

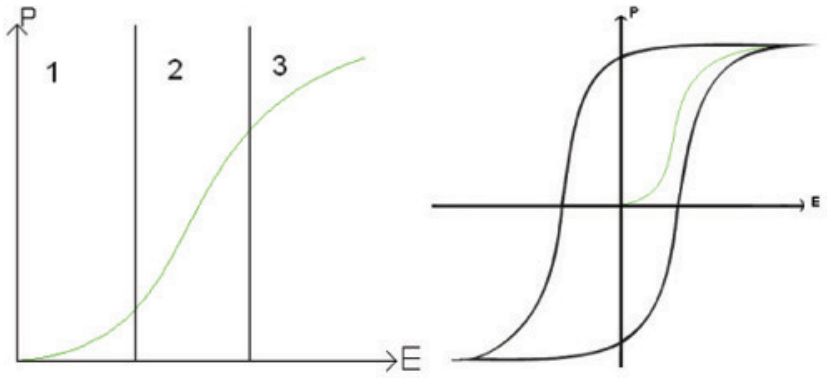

Figure 2.7 Illustration how minor hysteresis curve fits major hysteresis curve [28]

So, switch process compatible with previous Figures of 2.6 and 2.7 is illustrated in Figure 2.8, additionally.

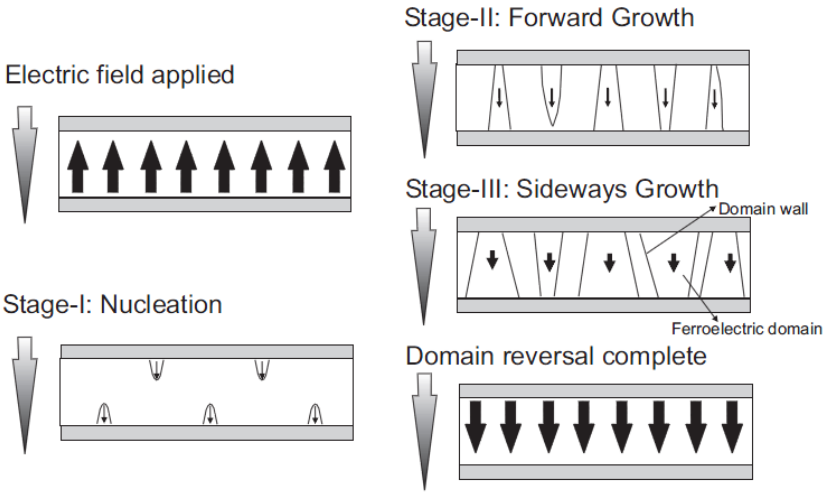

Figure 2.8 The domain switching stages, 1) Nucleation 2) Forward growth 3) Sideways growth [29]

The domains are the regions where a many dipoles have aligned below the Curie temperature. At the beginning, before electric potential is applied, the domains have randomly orientation which results in zero net polarization. In presence of external field, the domains of favorable directions orient parallel to electric field, those domains with compatible orientation get larger while the other domains diminish. This process of high voltage is called poling and poling is generally applied in Curie Temperatures [30]. The poling process is shown in Figure 2.9.

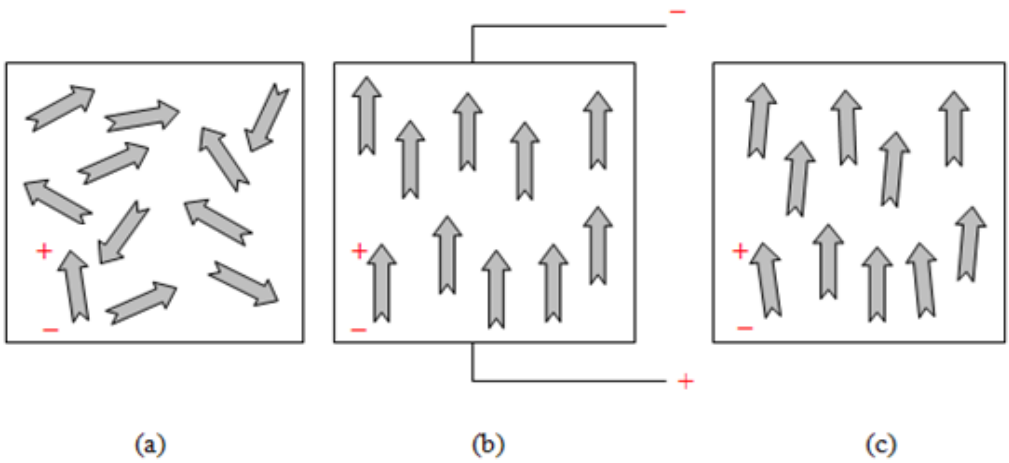

Figure 2.9 Direction of dipoles, (a) randomly orientation, (b) electric field applied, (c) remnant polarization [31]

2.2.2. Ferroelectric Thin Film Applications

Ferroelectrics have been commonly used in many applications, due to its properties such as piezoelectricity, polarizability, high permittivity, pyro-electricity, electro-optic activity (Figure 2.10). Currently, one of the main applications of ferroelectrics is memory applications. There are problems of read/write cycle times, and capacity for other memory devices. Many memory devices have been overcome by ferroelectric random access memories (FeRAM). Figure 2.11 shows architecture of high and low density FeRAMs.

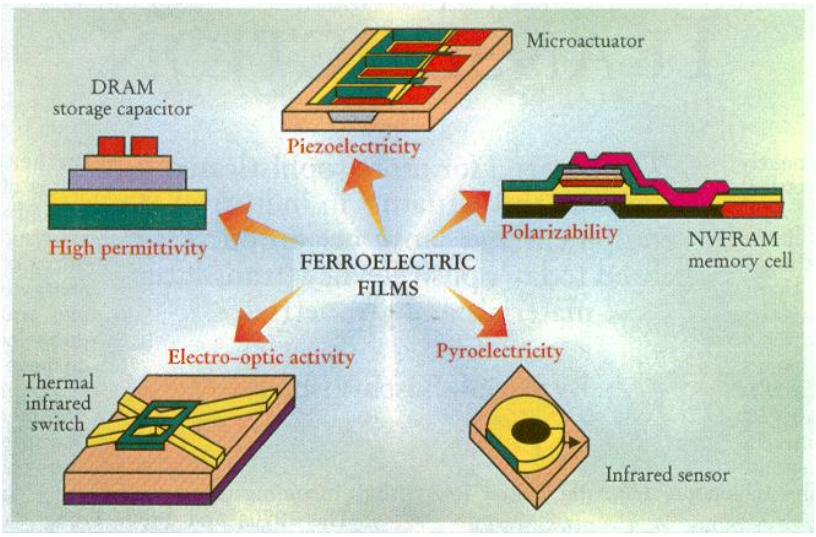

Figure 2.10 Applications of ferroelectric films [33]

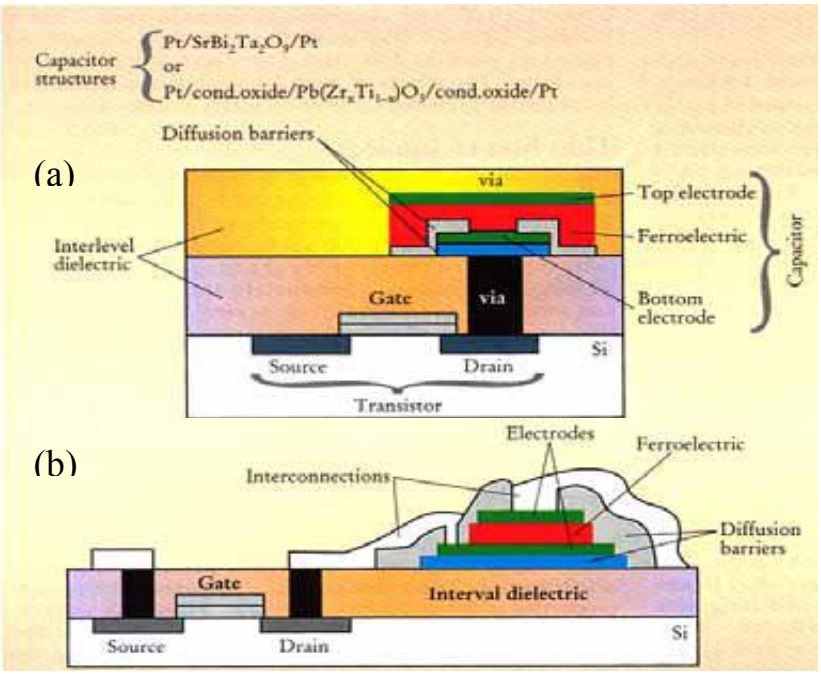

Figure 2.11 Illustration of FeRAMs (a) Vertical high-density FeRAM architecture (b) Lateral low-density FeRAM Architecture [34]

In Ferroelectric RAM, which is also called FeRAM, F-RAM or FRAM, ferroelectric layer is used to store data non-volatile. Remnant polarization is used to store data. Nowadays, mass production of FeRams with read/write cycle times in the smaller

than 100 ns range and small voltage requirements. For example, 0.5 μm, low-density with 4-256 kbytes FeRAM has access time of 120-70 ns while 0.13 μm, high-density with 4-64 Mbytes FeRAM which has crystal-oriented-particles (COP) has access time of 45-15 ns [35]. An important factor is the thickness of ferroelectric film. Generally, ferroelectric domains can be switched if the film thickness is lower than 1 μm [36].

2.3. Piezoelectric Properties of Materials

Certain crystals, for example quartz, barium titanate and lead zirconate titatanate can be polarized under mechanical forces. The mechanical forces provide appearance of surface charges results in electrical potential difference of two surfaces of the crystal. These crystals also exhibit mechanical strain or distortion when electric field is applied. Piezoelectricity can be defined by these two effects define piezoelectricity. In Figure 2.12, (a) the condition when no voltage or stress applied (b) the voltage generated by strain, (c) compression due to voltage (d) extension due to voltage of a piezoelectric material are demonstrated [37].

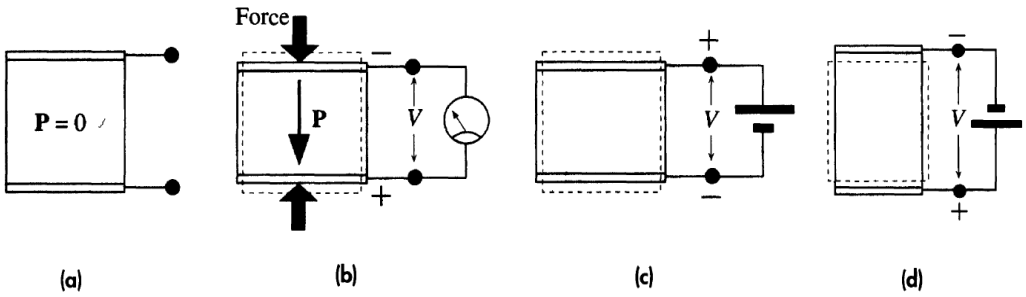

Figure 2.12 The piezoelectric effect of a crystal

2.3.1. Piezoelectric Materials Applications

Lead zirconate titanate (PZT) which is to be soon prohibited is most commonly used piezoelectric material. In lead zirconate titanates, 0.1% change in original dimensions can be provided by applied voltage. Even at first glance this percentage seems relatively small; it is sure enough to produce ultrasonic sensor which is one of main

application areas of piezoelectric materials. The strain gages, sonar detectors, energy harvesting devices and MEMs are some of the areas where piezoelectric materials are employed [38].

There are four main applications of piezoelectric ceramics:

- Piezoelectric Generator: generates voltages sufficient to start spark formation between an electrode gap.
- Piezoelectric Sensor: transforms physical change into signal.
- Piezo Actuator: converts signal to physical change.
- Piezoelectric Transducer: transforms electrical energy into vibrational mechanical energy [39].

2.3.2. Piezoelectric Charge Constant (d)

Dielectric displacement or total surface charge density D, which was expressed in Equation 2.9 can also be defined by the piezoelectric charge constant, d.

The direct piezoelectricity,

$$D = dT + e^{T}E \qquad \text{Eq. [2.11]}$$

$$d = D/T \qquad \text{Eq. [2.12]}$$

where D represent dielectric displacement, T represents the applied stress on piezoelectric material [40].

By equating the Equation 2.12 dielectric displacement D (Coulombs/Area) with applied stress on the piezoelectric material, T (Force/Area), piezoelectric charge constant is defined in

$$d = \text{Coulombs}/\text{Force}$$

equation. Direct piezoelectric coefficient is used in most of bulk applications and generally pC/N is the widely used unit of piezoelectric charge constant. For instance,

the piezoelectric coefficient for BCT-BTS bulk material was reported 530 pC/N at mostly [14].

The reverse piezoelectricity effect is defined by mechanical deformation (e.g. extension or compression) occurs due to movement of atoms in the piezoelectric material due to applied electric field [40]. In this situation, the physical change is expressed as,

$$S = dE + s^{E}T \qquad \text{Eq. [2.13]}$$

$$d = S/E \qquad \text{Eq. [2.14]}$$

where S represents the strain on the piezoelectric material [24,25].

Strain of the piezoelectric material is,

$$S = \Delta L/L \qquad \text{Eq. [2.15]}$$

Electric field is,

$$E = V/m \qquad \text{Eq. [2.16]}$$

Hence, by equating the equations, Equation [2.15] and [2.16] to the Equation [2.14] we can obtain

$$d = \text{Meter/Volt} \qquad \text{Eq. [2.15]}$$

In order to measure piezoelectricity of thin films due to incapability and uselessness of applying force to a thin film. Instead of applying mechanical force on piezoelectric thin films electric field is applied. The piezoelectric constants of typical PZT thin films around 500 nm varies between d~90-110 pm/V [41].

2.3.3. Piezoelectric Voltage Constant (g)

The piezoelectric property also can be expressed by the piezoelectric voltage constants, g coefficient in volts/meter per Newton/square meter. For instance, a typical PZT has the piezoelectric voltage constant of 24.6 mmV/N [42].

2.3.4. Electromechanical Coupling Factor (k)

The electromechanical coupling factor, k, can be expressed by terms of k^2

$$k^2 = \frac{\text{electrical energy converted to mechanical energy}}{\text{input electrical energy}} \qquad \text{Eq. [2.16]}$$

or equivalently by,

$$k^2 = \frac{\text{mechanical energy converted to electrical energy}}{\text{input mechanical energy}} \qquad \text{Eq. [2.17]}$$

The electromechanical coupling factor, k represents efficiency of piezoelectric material to transform electrical energy to the mechanical energy or vice versa. k does not have dimension and it can not be higher than 1, because the transformation of mechanical energy to electrical energy has losses. One of highest k has a value of 0.8 [43]. The k of BCT-BTS bulk piezoelectric is 0.55 [14].

2.4. State of Art

Presently, FeRAMs are widely used in electronics due to low power consumption, read/write speed and capacity [42]. In addition to this, piezoelectric thin films are used in MEMs which possess a huge and growing market. According to regulations mentioned in previous parts, the lead free materials in thin film form have been researched increasingly over the last decade. On the other hand, these studies herald existence of microstructural fabrication problems. This thesis aims production of thin film with a highly probability to be an alternative to lead based materials, briefly.

Generally, alternatives to lead based compositions are categorized as three main families.

2.4.1. Potassium Sodium Niobates

The first alternative family, the potassium sodium niobates (KNN) exhibit high Curie temperature, adequate ferroelectric properties, and high values of electromechanical coupling factor. Actually, standard of piezoelectric coefficient for pure KNN structures are around 100 pC/N. For this reason, compositional modifications including Li, Ta, Sb, Ta addition have been done for enhancement of piezoelectric response. The piezoelectric coefficient of KNN compositions reached values higher than 400 pC/N with modifications in $(K,Na,Li)(Nb,Ta,Sb)O_3$ phases, however average values are between 100 to 250–300 pC/N [44-45]. These numbers are comparable with 200–600 pC/N in commercial PZT. Saito et. al. has achieved the highest piezoelectric coefficient of 416 pC/N with composition of $(K_{0.44}Na_{0.52}Li_{0.04})(Nb_{0.86}Sb_{0.04}Ta_{0.10})O_3$ [44]. Zhou et. al. has studied optimal sintering temparture for Li-modified $(Na,K)NbO_3$ ceramics, $(1-x)KNN-xLiSbO_3$ and achieved piezoelectric coefficient of 286 pC/N with an efficient electromechanical coupling factor of 0.51 at x=(4.8-5.6)% [46]. Moreover, the MPB has been obtained with (1-x)KNN-xLT at x=5-6 mol.% in a study [47].

KNN based lead-free compositions are studied by researchers in order to possess new systems. A significant problem is densification problem. This problem is partially solved by the researchers [48]. Even though the electrical responses are comparable with PZT, this family is still not enough to be an alternative to PZT.

2.4.2. Bismuth Sodium Titanates

Another family, bismuth sodium titanates (BNT), perovskite ferroelectric have also been considered as a strong alternative. BNT has a relatively high T_C of 320°C, piezoelectric coefficient 73 pC/N and remnant polarization 38 $\mu C/cm^2$. Another advantage of BNT is the ease of fabrication because mainly precursors do not contain

volatile content and lower sintering temperatures compared to KNN based ceramics. However, BNT piezoelectric have large coercive field (70 kV/cm). Moreover the conductivity is high that results in inadequate poling. Also MPBs of BNT-based solid solutions are temperature dependent boundaries. In addition to these, BNT-based system phase diagram has low depolarization temperature, T_d above which piezoelectricity vanishes.

Due to these reasons, it was essential to seek alternatives for BNT based solid solutions to possess high piezoelectric performance so that numerous modifications have been done in composition and production methods for enhancement of piezoelectric response. MPB region in (1-x)BNT-xBT system at x=0.06-0.07 with T_C of 288°C and T_d 130°C was studied [49]. $[Bi_{0.5}(Na_{1-x-y}K_xLi_y)_{0.5}]TiO_3$ (BNKLT) phases were developed. The results of this study showed that this phase has piezoelectric coefficient 231 pC/N, electromechanical coupling factor of 0.41 which is relatively where electromechanical properties can be optimized with composition of x=0.15 and y=0.075 [50]. Hiruma et. al. proved that Li-substitution (0.04) helps significantly to increase T_d. For BNT-BKT-BLT ternary system T_d increased to 221°C [51]. Even though BNT based ceramics are under global attention, due to thermodynamic restrictions of ternary systems of BNT based solid solutions which is non-existence of tricritical point, BNT based ceramics are not good alternatives to lead based ceramics.

2.4.3. Barium Titanate Based Compositions and BTS-xBCT System

Another lead-free alternative family is $BaTiO_3$ and $BaTiO_3$-based solid solutions. $BaTiO_3$ was the first material that piezoelectricity was discovered and used in radars in World War II. The high dielectric constant in the $BaTiO_3$ compositions was found by Thurnauer [52].As time went by, lead zirconate titanate dominated the market. For more than five decades, $BaTiO_3$ and $BaTiO_3$-based solid solutions have been accepted as good dielectric materials but relatively low piezoelectric response of $BaTiO_3$ kept it as a non-alternative for lead-free materials. Recent studies have shown that high piezoelectric response can be obtained by the whether the phase has a triple point (tricritical point). This point should have be the intersection point of

paraelectric cubic phase (C), ferroelectric rhombohedral (R) and tetragonal phases. Such a phase boundary (tricritical triple point type) has a flattened energy landscape and consequently lower energy barrier for polarization switching. So moving closer to triple point (C-R-T) is favorable for polarization rotation. According to this fact, triple point temperature should be lowered to working temperatures in order to promote polarization. The doping of either A or/and B site substitutions decreases the tricritical point temperature. For example, in the $BaTiO_3$ based systems the addition of Ca^{+2} into barium site decreases tricritical point temperature [53-54]. One should be very careful about the relation between working temperature and tricritical point temperature, while moving of working temperature closer to tricritical point promotes polarization, it also has the potential to cause depolarization, because if the tricritical point is exceeded then the material will be paraelectric and ferroelectricity will be vanished.

Up to very recent years only $BaTiO_3$-based BZT-xBCT system was reported to possess both triple point and high piezoelectricity. As result of studies with optimal composition of BZT-xBCT, in $(Ba(Zr_{0.2}Ti_{0.8})O_3$-$0.5(Ba_{0.7}Ca_{0.3})TiO_3$ piezoelectric coefficient is up to 630 pC/N that can be accepted as higher than most of lead-based systems. On the other hand, whether a wider range of $BaTiO_3$-based systems with high piezoelectricity can be obtained was the question. So in Xue's study, researchers designed a lead-free, $BaTiO_3$-based composition, $Ba(Ti_{0.88}Sn_{0.12})O_3$-$x(Ba_{0.7}Ca_{0.3})TiO_3$. In this study, Xue's team has managed to have piezoelectric coefficient of 520 pC/N. In Figure 2.13, comparison of this system with some lead-free and lead-based commercial ceramics can be seen.

In this system two compounds, $Ba(Ti_{0.88})Sn_{0.12}O_3$ (BTS) and $x(Ba_{0.7}Ca_{0.3})TiO_3$ (BCT). All the samples had $BaTiO_3$ like perovskite structure and BTS and BCT are characterized by R and T structure respectively. In Figure 2.14 (a) the phase diagram of BTS-xBCT is shown. Between Fig.s 2.14 (b) and (e) dielectric constant can be seen. This phase boundary start from C-R-T point at x=8 and at 47 °C temperature. In Figure 2.14 (f), the thermal hysteresis of C-T and C-R transition decreases sharply towards the triple point and nearly vanishes at that point. These facts suggest that this is a tricritical point. In 5BCT, a near-triple composition exhibits the highest dielectric

constant at T_C. Because this system possesses a tricritical point and a similar phase boundary with BZT-xBCT system, equally excellent piezoelectric properties are expected.

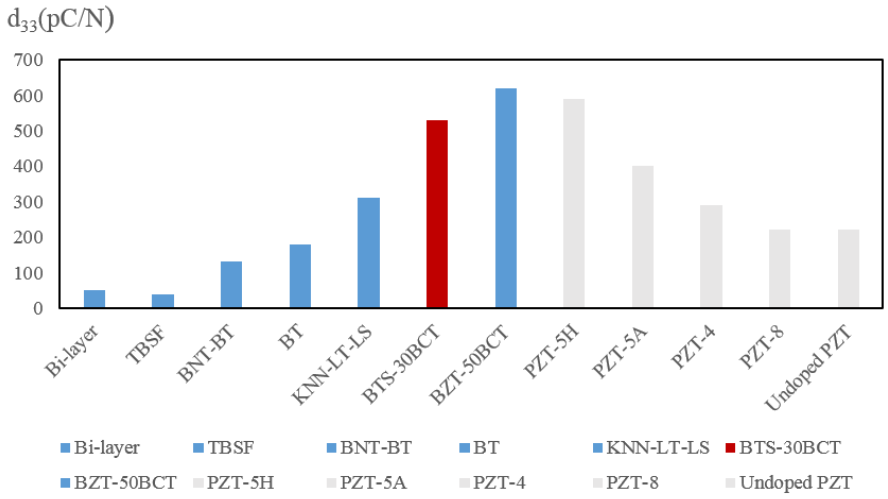

Figure 2.13 Comparison of piezoelectric coefficients for BTS-30BCT ceramic with some lead-free and lead based-commercial ceramics [19]

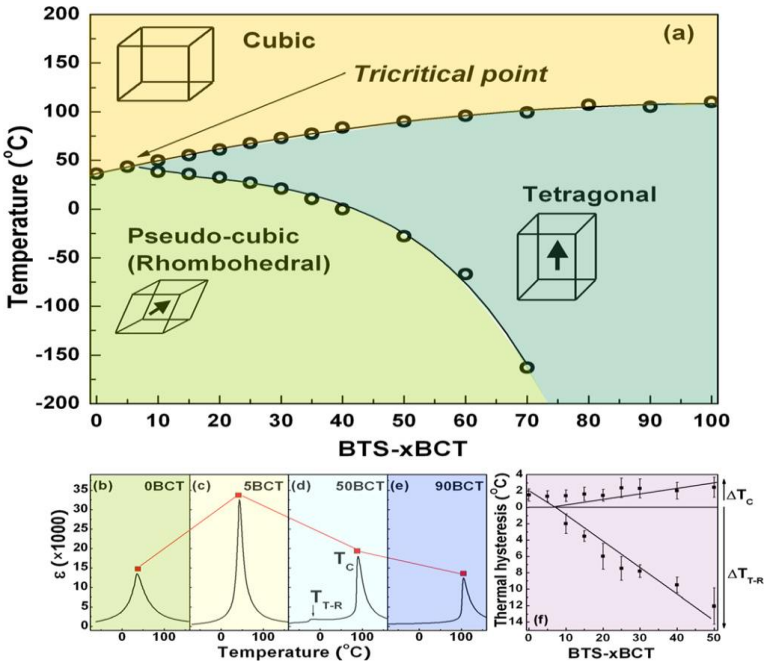

Figure 2.14 (a) Temperature-composition phase diagram of BTS-xBCT (b)-(e) Typical dielectric permittivity vs temperature curves for BTS-xBCT (x=0,5,50,90) (f) At tricritical point (about BTS-8BCT), transition thermal hysteresis of the three transitions vanishes [14]

Figure 2.15 reveals the composition dependence of properties of BTS-xBCT system at room temperature. As shown in the figure, the optimal composition is 30BCT which has fairly low E_C but the highest P_m, P_r and ε. The dielectric constant value of BTS-30BCT is about 3800, comparable with soft PZT materials (2000-3500) [55]. At BTS-30BCT d_{33} is maximum at 530 pC/N. The dS/dE reaches maximum 820 pm/V and this value is comparable with soft PZT ceramics (900 pm/V). In this composition E_C is relatively low, about 280 V/mm.

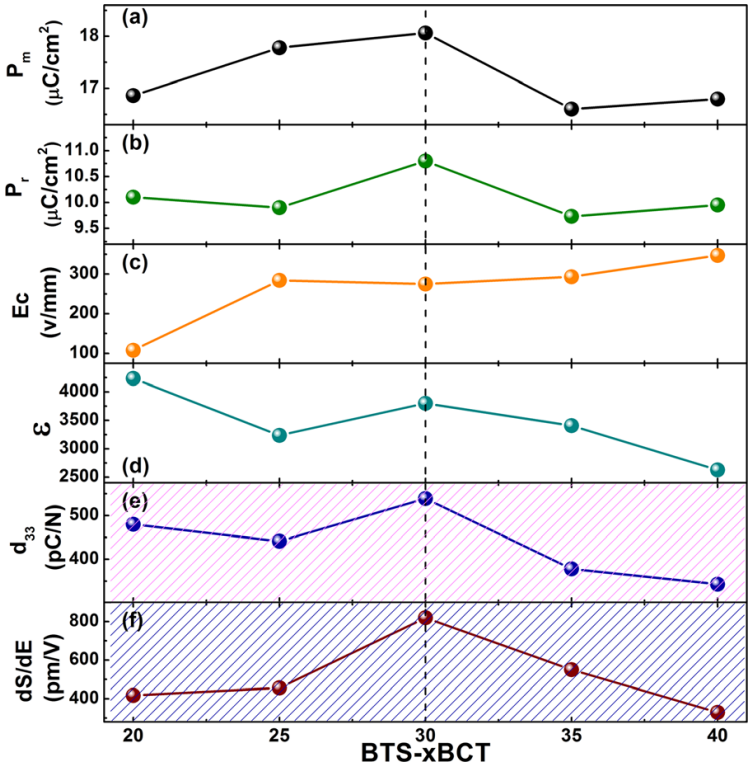

Figure 2.15 Composition dependence of (a) the saturation polarization P_m, (b)remanent polarization P_r, (c) coercive field E_C, (d) permittivity ε (e) piezoelectric coefficient d_{33}, and (f) converse piezoelectric coefficient dS/dE [14]

In order to reveal why such uncommon, high piezoelectric response for BTS-30BCT (530 pC/N) is present for a lead-free system, a composition related phase transition phenomenon for perovskite oxides should be understood. In perovskite oxides phase diagrams, the transition line is morphotropic phase boundary (MPB) which seperates rhombohedral and tetragonal phases. Actually, both of polarization directions for R <111> and T <001> exist in MPB. This coexistence of two polarization direction

causes the instability of polarization state which facilitates rotation of polarization direction by electric field [56, 57]. In Figure 2.16 polarization direction of tetragonal, rhombohedral and coexistence of tetragonal and rhombohedral phases may be seen. As it can be understood from the figures, in vectorial notation the most favorable direction for activating polarization of tetragonal phase is (111) while for tetragonal phase it is (100). Even though other lead-free families have MPB, it was not clear why their piezoelectric properties were lower than lead-based and $BaTiO_3$ based systems such as BTS-xBCT and BZT-xBCT. The important point here is the existence of tricritical point (TCR) in lead-based and $BaTiO_3$ based systems such as BTS-xBCT and BZT-xBCT.

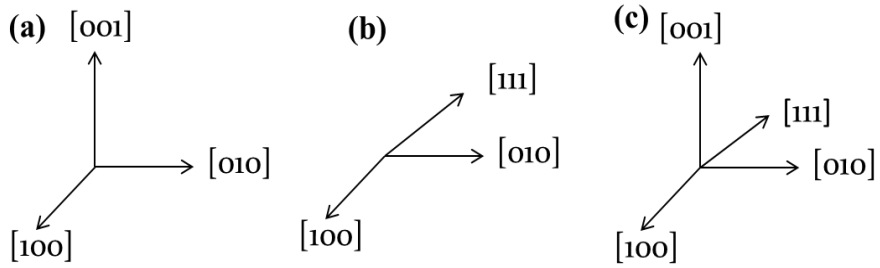

Figure 2.16 Illustration of polarization directions for (a) tetragonal phase, (b) rhombohedral phase, (c) coexistence of these two phases

The free energy (F) for polarization switching can be expressed in Landau polynomial (Equation 2.18), in terms of temperature (T), composition (x), polarization magnitude (P) and direction of polarization (n) [58].

$$F(x,T,n,P) = A(x,T)P^2 + B(x,n)P^4 + C(x,n)P^6 \qquad \text{Eq. [2.18]}$$

where A(x,T), B(x,n), and C(x,n) represent second, fourth, and sixth order term coefficients, respectively. In the situation that the composition is precisely on triple point, $B(x_{MPB},n) = B(x_{TCP},n) = 0$ and $C(x_{TCP},n) = C(x_{TCP})$ condition should be provided. Then, the Equation 2.18 simplifies to,

$$F(x_{TCP},T,n,P) = A(x_{TCP},T)P^2 + C(x_{TCP})P^6 \qquad \text{Eq. [2.19]}$$

Consequently, polarization direction has no effect on the free energy for polarization

rotation if and only if the composition is precisely on the tricritical point. The isotropy provides zero energy barrier for polarization rotation. This is reason for the main difference between the piezoelectric properties between MPB possessing phases, the phases with or without tricritical point. As mentioned before, the relation between working temperature and tricritical point temperature is extremely important, while moving of working temperature closer to tricritical point promotes polarization, in the situation tricritical point temperature is exceeded then the material will be paraelectric. However, even production of phases on MPB close to tricritical point will dramatically increase the polarization. This time the free energy for polarization rotation will not be zero but still polarization direction will have very limited effect so that polarization rotation will be still easy.

In the free energy diagrams of Figure 2.17, the free energy difference between the phases which have tricritical MPB such as BTS-xBCT or PZT, and the phases without tricritical point MPB such as KNN or BNT can be observed clearly. In systems with Polymorphic MPB, anisotropy results in larger energy barrier for polarization which leads to lower polarization when compared with tricritical MPB systems which are nearly anisotropic. Hence, this comparison explains the difference in piezoelectric properties between tricritical point type MPB phases such as BTS-30BCT (d_{33}~ 530 pC/N) and PZT (d_{33}~ 600 pC/N) and others phases without tricritical point MPB (d_{33}~100-350).

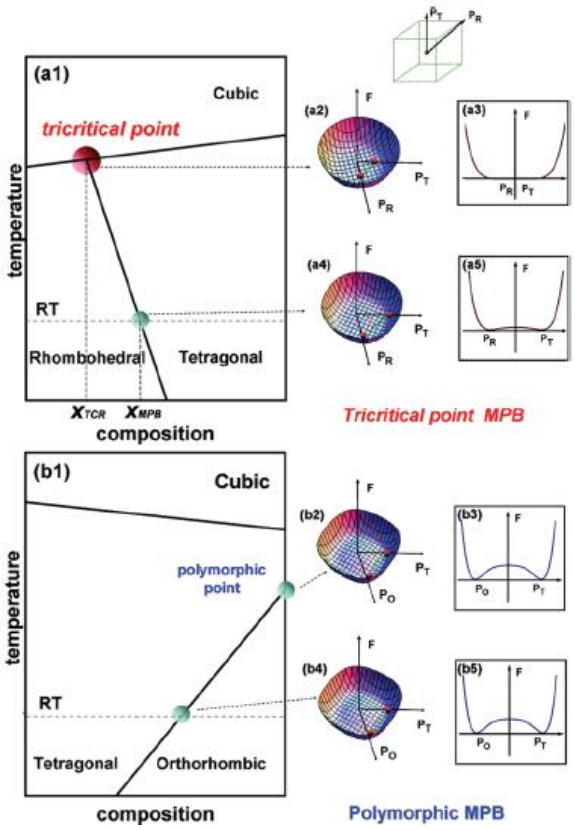

Figure 2.17 (a1) Illustration of a triple point MPB between tetragonal (T) and rhombohedral (R) phases. (a2), (a3) Isotropic free energy surface for triple point. (a4), (a5) Free energy very close to isotropic free energy surface of MPB composition at RT (b1) Illustration of a polymorphic MPB between (T) and orthorhombic (O) phases. (b2), (b3) Illustration of anisotropic free energy surface for polymorphic point. (b4), (b5) Illustration of anisotropic free energy surface for polymorphic MPB at RT. [19]

2.4.4. Development of Lead-Free Thin Films

The main problem of lead-free thin films is to obtain high-quality films. KNN-based and BNT-based thin films contain volatile elements content such as K^{+}, Na^{+}, Bi^{3+}, Ti^{4+} while BT-based thin films contain Ti^{4+}. Most probably a non-stoichiometric thin film is obtained due to volatile content in compositions. As mentioned before, stoichiometry is extremely important for enhancement of electric properties, so that total control of the fabrication parameters is required [45].

For KNN-based thin films, different fabrication techniques exist such as RF magnetron sputtering, metal-organic chemical vapor deposition (MOCVD), sol-gel deposition, and pulsed laser deposition (PLD) [45]. Especially for KNN-based thin films, most probably a non-stoichiometric thin film is obtained because the volatile content in KNN are light which cause tendency to have thermalization problem in addition to other problems due to volatilization. The volatilization of monovalent species (K^+, Na^+) results in higher conductivity that decreases ferroelectricity. This problem have been tried to be solved by ensuring proper oxygen stoichiometry. Applying O_2 gas pressure during fabrication preserves film stoichiometry. If volatilization of A-site cations can be suppressed, domain wall mobility enhancement and reduced E_C can be obtained. Moreover this suppression provides a higher A-site/B-site cation ratio [59]. These type of KNN-LT-LS thin films having Li content possess longitudinal piezoelectric coefficient, d_{33}~53 pm/V [60]. Addition of 5mol%LN in NKN exhibited P_r and E_C values 10 $\mu C/cm^2$ and 45 kV/cm, respectively [61]. In the study for optimizing $K_xNa_xNbO_3$, $K_{0.55}Na_{0.55}NbO_3$ composition showed typical ferroelectric hysteresis and field-induced strain loops. The P_r and E_C values were 7.0 $\mu C/cm^2$ and 70 kV/cm respectively. The effective d_{33} was found to be 46 pm/V [62]. By RF magnetron sputtering pure KNN films with high degree of (100) preferred orientation have been produced. The dense columnar structure resulted enhanced remnant polarization of Pr=12.0 $\mu C/cm^2$. These thin films exhibit high coercive field of ~100 kV/cm [63]. By pulsed laser deposition, on platinized substrates highly columnar structure with $(K_{0.44}Na_{0.52}Li_{0.04})(Nb_{0.84}Ta_{0.10}Sb_{0.06})O_3$ composition were deposited, exhibiting P_s = 3.8 $\mu C/cm^2$ and E_C = 20 kV/cm [64].

Bismuth sodium titanate based compositions have also been studied in thin film form. BNT-based thin films can be produced by different production methods comparable with KNN. Sol-gel method is again a common method. In 0.9BNT-0.1BKT thin films, remnant polarization and coercive field were found P_r~8.3 $\mu C/cm^2$ and 200 kV/cm respectively [65]. Thin films with polycrystalline structure of $[Bi_{0.5}(Na_{0.7}K_{0.2}Li_{0.1})_{0.5}]TiO_3$ (BNLKT) were grown by PLD, exhibited P_r of 13.9 $\mu C/cm^2$, a coercive field E_C of 102 kV/cm and piezoelectric coefficient d_{33}~ 64pm/V [66]. Enhanced $(Bi_{0.5}Na_{0.5})_{0.94}Ba_{0.06}TiO_3$ thin films, P_r of 29.5 $\mu C/cm^2$ and d_{33}~ 31pm/V have been obtained by La+Ce doping where Mn doping seems more favorite

to reduce the leakage current by two order of magnitude [67]. Moderate piezoelectric response for BNT-based composition have been obtained by sol-gel process of $Bi_{0.5}(Na_{0.85}K_{0.15})_{0.5}TiO_3$ composition. The effective piezoelectric coefficient of this phase was d_{33}~75 pm/V. The piezoelectric responses of the films were mainly promoted due to MPB composition. However the remnant polarization of these films were relatively low, $P_r = 7\ \mu C/cm^2$ [68].

BT-based thin film fabrication methods are same with other lead-free families. $BaTiO_3$ nanocrystalline thin films were produced by RF magnetron sputtering with remnant polarization and coercive field of P_r=5 $\mu C/cm^2$ and E_C=1.5 kV/cm respectively [69]. By sol-gel process, $Ba_{0.8}Sr_{0.2}TiO_3$ (BST) thin films were fabricated that exhibit remnant polarization P_r of 2.5 $\mu C/cm^2$ and coercive field E_C of 20 kV/cm with dielectric constant of 794 [70]. Xiao et. al. showed the relation between annealing temperature and ferroelectric properties in the barium strontium titanate thin films. At annealing temperature of 800 °C, $Ba(Sn_{0.15}Ti_{0.85})O_3$ film possessed an increased properties such as remanent polarization and coercive field values 4.57 $\mu C/cm^2$ and 76.1 kV/cm respectively, rather than lower annealing temperatures of 600 °C and 700 °C [71]. In another study $Ba(Sn_{0.15}Ti_{0.85})O_3$ (BTS) thin films were coated on platinized silicon substrates by sol-gel method with a 30 nm BTS seed layer. In this study, permittivity of with and without seed layers were found as 720 and 395, respectively. So that seed or buffer layers have important impact on these films [72]. By using same composition of BTS films, 0.1 and 0.4 M solutions indicated that tunability of these solutions with different molarity were 54% and 25% under 200 kV/cm, respectively [73]. In $(Ba,Ca)(Zr,Ti)O_3$ derivatives, a significant study was done by Lin et. al. that investigated $(1\text{-}x)Ba(Zr_{0.2}Ti_{0.8})O_3 - x(Ba_{0.7}Ca_{0.3})TiO_3$ thin films. The films had random orientated grains and adequate permittivity from 350 to 500 and a low tangent loss about 3%. At x=0.55 the films exhibited a remanent polarization P_r of 2.81 $\mu C/cm^2$ and coercive field E_C of 33.73 kV/cm [74]. By PLD, $[Ba(Ti_{0.8}Zr_{0.2})O_3]$-$[(Ba_{0.7}Ca_{0.3})TiO_3]$ dense and oriented films were deposited which exhibited remnant polarization, dielectric constant and piezoelectric coefficient of 14.1 $\mu C/cm^2$, 1010 and 80 pm/V, respectively. These results are higher than sol-gel fabricated thin films due to existence of porosity in sol-gel fabricated films that acts as moisture source which causes ionic conductivity

on the surface [75]. In the thesis study of Çeltikçi, $Ba(Ti_{0.8}Zr_{0.2})O_3$-$(Ba_{0.7}Ca_{0.3})TiO_3$ composition thin films annealed at 800 ^oC exhibited remanent polarization and coercive field values of 2.9 $\mu C/cm^2$ and 49.4 kV/cm respectively. Additionally, the permittivity of 356 and a tangent loss of 3.52% at frequency of 600 KHz were obtained [76].

In this thesis $BaTiO_3$-based system, $Ba(Ti_{0.88}Sn_{0.12})O_3$-$0.3(Ba_{0.7}Ca_{0.3})TiO_3$ (BTS-BCT) thin films have been fabricated by sol-gel technique.

2.5. Sol-gel Technique

In sol-gel method alkoxide precursors, primarily hydrolysis and polycondensation take place, are used which provides a remarkable fabrication technique that scientists have used it for more than one century to fabricate various materials. Powders, films, monoliths, dense ceramics, aerogels and fibers can be produced by this technique (Figure 2.18) [77]. In the sol-gel process, molecular precursors are transformed into nanometer-sized particles to form a sol, or colloidal suspension. With sol-gel fabrication technique, a broad set of materials for applications such as opting coating, energy storage, ceramics, waste remediation and nanoelectronics.

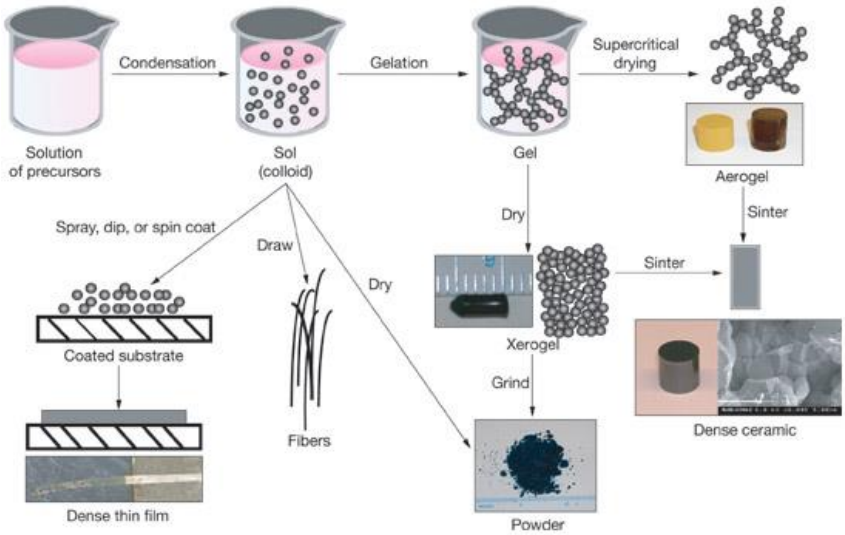

Figure 2.18 Steps of sol-gel technique for synthesis of different materials [77]

For electronics, sol-gel technique exhibits many advantages such as purity, homogeneity, low temperature processing, ease of a broad range of production, and unique properties directly related with the process.

Sol-gel process is composed of wet chemical reactions. The molecular precursors are in solution form that enables the distillation of the materials. In this manner, high purity materials can be used to fabricate electronic ceramics. In addition to this, the existence of individual elements in liquid form results in mixing at atomic level. Thus more homogeneous final material is obtained. At colloid formation step, films can be easily coated on substrate, fibers can be drawn and powders can be formed due to fluid state of material. If colloid formation step is followed by gelation, then the gel is porous. The pores have nanometer-level (10 nm) diameter. This situation allows relatively low temperature processing. These low drying temperatures help to overcome undesired phase transitions, and volatilization problems. Provided by the options available in steps of sol-gel process, porosity, crystal structure, and grain size can be controlled quite well. Hence a broad range of compositions and structures can be formed which enables unique properties of the material which is sol-gel derived only [78].

2.5.1. Preparation of the Solution

Figure 2.19 shows typical chemical solution deposition (CSD) process to fabricate thin films with perovskite microstructure.

The CSD process begins by preparing the proper precursors such as salts, carboxylates or other metallo-organic compounds, generally alkoxides. The proper solvents dissolve prepared precursors and the solutions are combined together with stoichiometry which will enable to produce the thin film with specific composition. The presence of volatile raw materials such as Ti-isopropoxide, Tin-isopropoxide, Pb-acetate should be considered in order to obtain the desired stoichiometric ratio. In addition to this, the complete dissolution of the precursors in solvents is an important factor that the homogeneity can be obtained for better film quality. Chemical stabilizers, if needed, may be added to produce crack-free films.

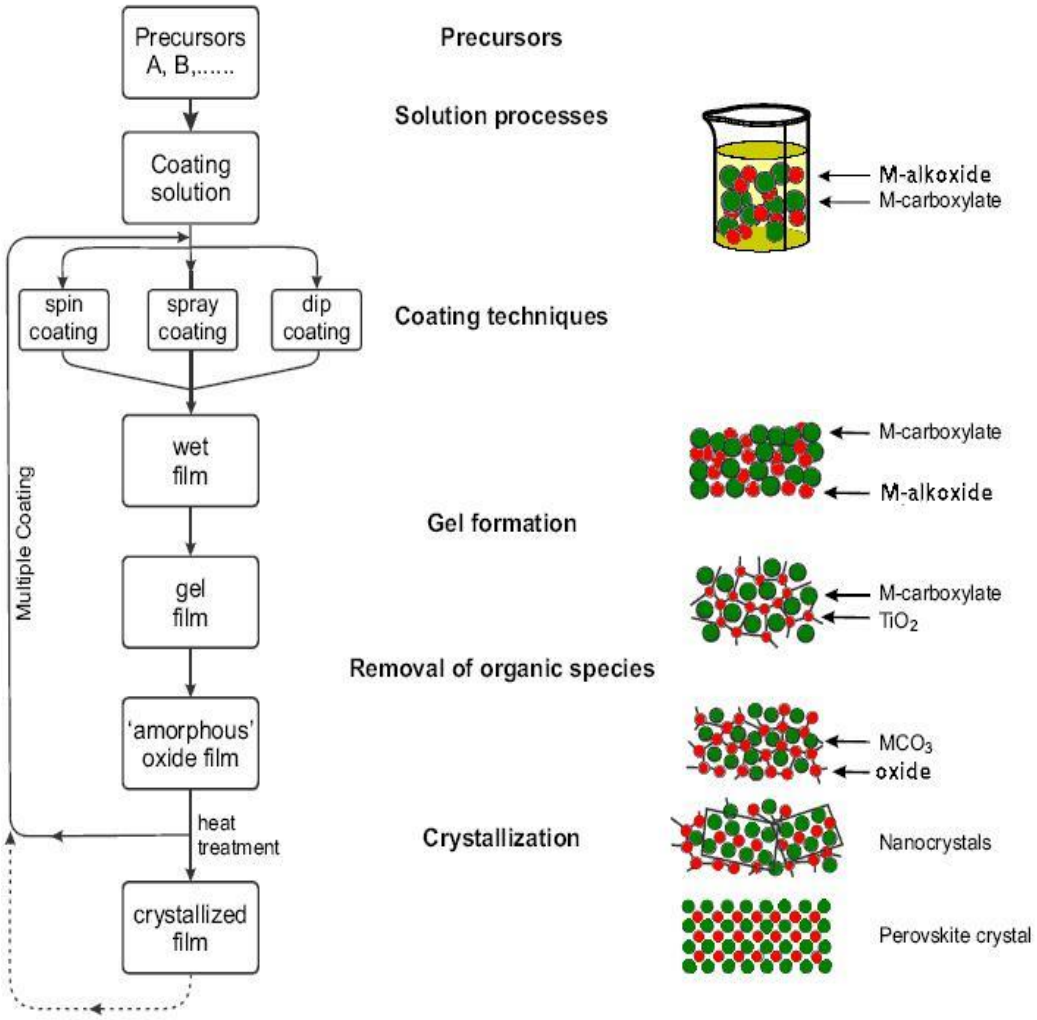

Figure 2.19 Flow chart of fabrication of perovskite thin film by chemical solution deposition (CSD) process [79]

In hydrolysis and condestation of alkoxides, metal salts of alcohol M-$(OR)_x$, metal part is M and alkyl group R are used.

Hydrolysis:

$$M(OR)_x + H_2O \longrightarrow M(OH)_x + {}_xROH \qquad \text{Eq. [2.20]}$$

Condensation :

$$2\ M(OR)_x(OH) \longrightarrow M_2O(OR)_{2x-3}(OH) + ROH \qquad \text{Eq. [2.21]}$$

Condensation :

$$2\ M(OR)_x(OH) \longrightarrow M_2O(OR)_{2x-2}(OH) + H_2O \qquad \text{Eq. [2.22]}$$

Metal-oxygen-metal links are structures that give the fundamental strength of oxide ceramics are formed due to these reactions. If the process continues, the solid network will grow until gelation or precipitation takes place.

2.5.2. Spin Coating Process

After preparation of the solution, there are three main coating techniques for perovskite thin film fabrication by chemical solution deposition; spin coating, spray coating and dip coating. Spin coating technique is most widely used in most of the researches due to ease in control, homogeneity and high quality film productions. Platinized silicon substrates are also the most widely used substrates for this technique. In spin coating, the substrate is put on the coater in vacuum or with the help of double-sided sticker. To obtain desired thickness, the spin rate of the spin coater (in rpm) and time can be adjusted. The rate and time of the spin and the molarity of the solution are directly related with the final film thickness. For instance, solutions with 0.4 M coated by 2250 rpm for 30 s results in ~40 nm layer thickness. The thickness of one coating layer or total thickness of the film can be predicted by considering Mayerhofer's equation

$$h\ \alpha\ f^{-2/3}\ \eta_i^{1/3}\ e^{1/3} \qquad \text{Eq. [2.23]}$$

where f is spin rate, η_i is the initial viscosity, and e is the evaporation rate.

Before coating, usually nozzled filters are used to clean precursor solutions from possible dirt containment and the coatings are done in clean rooms to maintain the cleanness of the solution.

The first step of spin coating can be considered as depositon. Generally excess amount of solution is dropped by pipe in order to have complete wetting of the substrate surface. The next step is to spin-up provides fluid expulsion from the substrate by rotational speed adjusted by the controller. The third step is spinning with a constant speed which results in the smoothing of the precursor. In the final step, evaporation of solution and start of the gel formation occur. The thickness and smoothing of the films are determined on the final step [80].

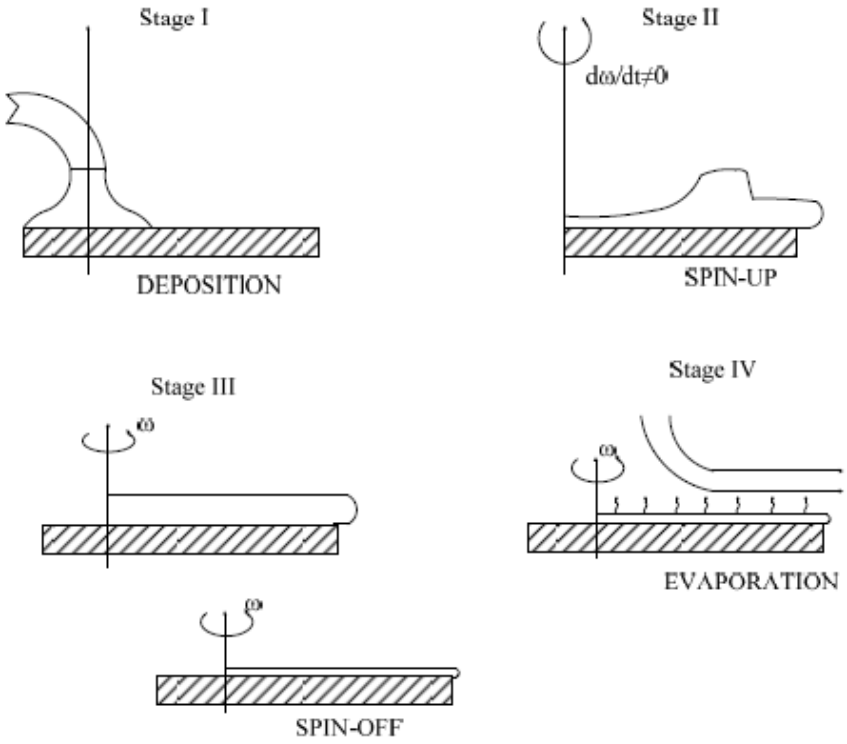

Figure 2.20 Stages during spin coating process [80]

2.5.3. Heat Treatment of Thin Films

As films are coated, drying at relatively low temperatures (~200 °C) is applied in order to eliminate water and solvent in the solution. The timing of the drying is important that cracking is very common in this step. In the beginning of drying step, the gel consists of two phases, the crosslink of solid phase and pores filled with liquid phase. The surface of the gel is covered with liquid phase. As the liquid phase evaporates, solid phase exposes. Since the solid network is completely wet due to liquid, as the liquid phase evaporates, the gel shrinks under capillary force. 50 - 70% of film thickness vanishes due to shrinkage. This situation results in cracks [81].

A well-studied thermal analysis should be done to select the proper temperatures for crystallization of the films. The most common approach for crystallization consists of two-step heat treatment process. The first step (pre-sintering) involves low-temperature pyrolysis (500°C) while the second step is high-temperature crystallization sintering (700-850°C). This two-step approach helps to form crack-free films because it is very likely that the rapid heat treatment causes cracks.

The carbonate phases form during heat treatment of $BaTiO_3$ based compositions. These formations cause some complexity in the process. Some of these complexities can be seen below:

- The formation of barium carboxylates at relatively high temperatures 450-500°C) that causes proper treatment time in pyrolysis step.
- The formation of secondary phases in the film which are generally complex carbonates, intermediate phase of $Ba_2Ti_2O_5CO_3$. These phases result in higher sintering temperatures for obtaining desired perovskite phases.
- The tendency of titanium isopropoxide to form titanium at 350 °C cause formation of titanium oxide intermediate phases and limited amount of alkaline carboxylate crystallite network [82-84].

2.6. Viscosity of the Solutions

Viscosity of a fluid expresses the inner friction of the liquid, in other words its resistance to flow. Deformation can be caused by either shear stress or tensile stress.

According to the distance **dy** enforced by two parallel plates, the viscosity **η** occurs due to the shear stress **τ**, and the velocity change **du**.

$$\eta\eta = \frac{\tau}{du/dy} \qquad \text{Eq. [2.24]}$$

where viscosity is represented as poises (P) or pascal-seconds (Pa-s); and 1 P is 1 dyne-s/sm^2 while 1 Pa-s is 1 N-s/m^2.

Provided by uniform flow, simply the shear stress **τ** can be expressed as,

$$\tau = \mu\frac{\partial u}{\partial y} \qquad \text{Eq. [2.25]}$$

where μ represents viscosity.

Generally fluids can be adapted to Newton's criterion. Newtonian and other types of fluids are drawn in Figure 2.21. The viscosities of Newtonian fluids are not affected by the shear rate.

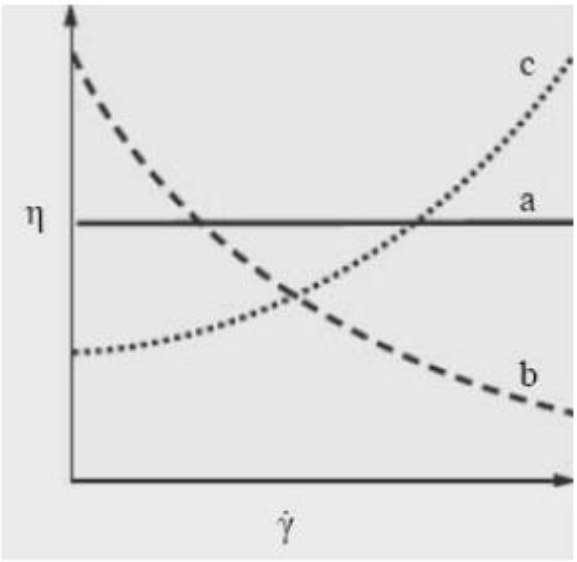

Figure 2.21 Different types viscosity of fluids (a) Newtonian (b) shear thinning and (c) shear thickening [76].

There exists a type of generalized Newtonian fluid as power-law fluid,

$$\tau = K(\frac{\partial u}{\partial y})^n \qquad \text{Eq. [2.26]}$$

where K represents flow consistency, n represents the flow behavior index [76].

Also the effective viscosity μ_{eff} can be obtained as a function of shear rate,

$$\mu_{eff} = K(\frac{\partial u}{\partial y})^{n-1} \qquad \text{Eq. [2.27]}$$

CHAPTER 3

EXPERIMENTAL PROCEDURE

In this research, $Ba(Ti_{0.88}Sn_{0.12})O_3-0.3(Ba_{0.7}Ca_{0.3})TiO_3$ (BTS-BCT) thin films were fabricated with respect to a nominal composition $(Ba_{0.91}Ca_{0.09})(Ti_{0.92}Sn_{0.08})O_3$. This composition was chosen near morphoptopic phase boundary (MPB) at room temperatures to maximize electrical properties. The thin film fabrication was carried out by preparing the solution, spin-coating, and heat treatment respectively.

3.1. Solution Preparation

3.1.1. Starting Materials

The starting materials necessary for precursor preparation of BTS-BCT film fabrication were barium acetate [$Ba(CH_3COO)_2$] (Alfa Aesar, purity 99+%), titanium *n*-propoxide [$Ti(OC_4H_9)_4$] (Aldrich , 97+%), tin (IV) isopropoxide [$Sn(OC_3H_7)_4$] (Alfa Aesar, purity 99+%), and calcium acetate hydrate [$Ca(CH_3COO_2)H_2O$] (Merck, purity 97+%).

In order to dissolve metal alkoxides and metal carboxylates, 2-methoxyethanol $C_3H_8O_2$ (Aldrich Co., purity 99%) and acetic acid $C_2H_4O_2$ (Merck Co., purity 100%) were utilized respectively. In order given, these solvents act as stabilizer and chelating agent additionally.

3.1.2. Solution Preparation

To prepare the homogeneous solution with the desired composition, two different solutions were prepared firstly. One of the solutions is composed of metal carboxylates (barium acetate, calcium acetate hydrate) and acetic acid while the other

solution is composed of metal alkoxides (tin (IV) isopropoxide, titanium *n*-propoxide) and 2-methoxyethanol. For metal carboxylates based solution, alkoxide powders (barium acetate, calcium acetate hydrate) with acetic acid solvent are combined and stirred by a magnetic stirrer at relatively high temperature, 125°C by using a hot plate. The high temperature prevents precipitation. For 1 h, the solution is mixed by using an oil bath and a reflux system. Reflux system prevents evaporation of the solution thus maintains molarity constant while oil bath provides homogeneous heating. Then the metal alkoxide based solution is prepared. The metal alkoxides (tin (IV) isopropoxide, titanium *n*-propoxide) and 2-methoxyethanol are mixed and stirred at RT (25°C) for 45 min. Once the two solutions are ready, they are mixed and stirred in reflux system at 80°C for 2 h time. In order to have a stable solution, the solution is stirred at RT for 1 day. After that the solution preparation is finalized. The final solution can be kept as a stock for several weeks if the crucible is ensured to be kept away from air. Before using the final solution for coatings, each time the solution was kept in ultrasonic bath for 15 min. The flow chart of the BTS-BCT film fabrication is arranged in Figure 3.1.

The amounts of starting materials were calculated. A low solute concentration, 0.4M was selected. The volume of the solutions prepared was 0.02 lt. In this manner, the starting materials total mole number of was 0.008. 0.905 gr barium acetate and 0.0566 gr calcium acetate were poured into pre-heated crucible containing 5ml acetic acid. This solution was stirred by magnetic stirrer in a reflux system at 125°C, for 1 h. Other precursors, titanium n-propoxide and tin (IV) isopropoxide had 10% excessive amount to compensate volatilization so that their amounts were 1.1522 gr and 0.1316 gr respectively. Titanium n-propoxide and tin (IV) isopropoxide were poured into 15 ml 2-methoxyethanol at RT. This solution was stirred by a magnetic stirrer for 45 min. Once both of the solutions are ready, they are mixed and stirred in reflux system at 80°C for 2h. The final solution should be absolutely transparent in order to be ensured to have a solution that all precursors were dissolved. At the end, for aging step, the final solution was stirred for 1 day at RT.

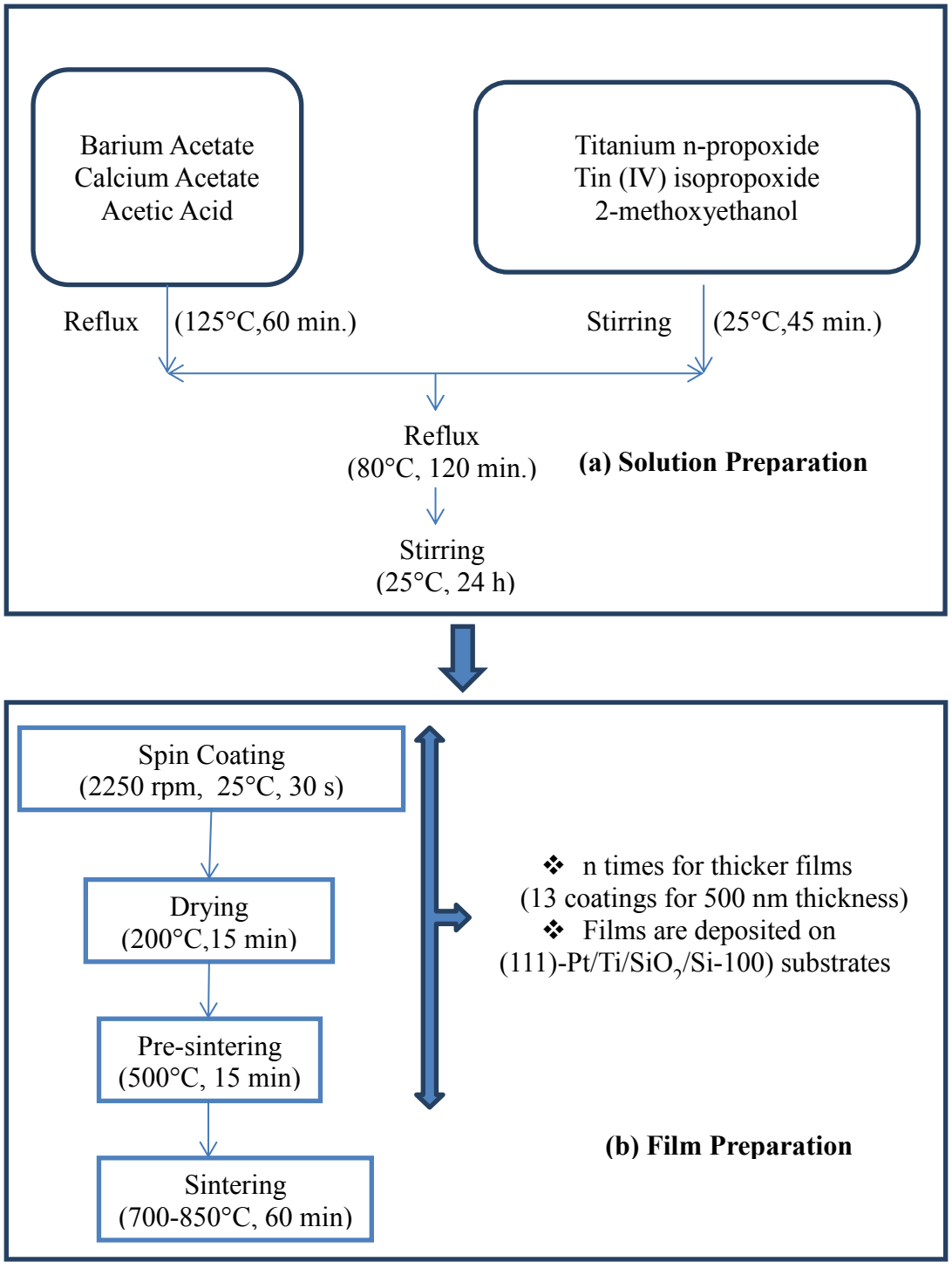

Figure 3.1 Flow chart for production of BTS-BCT thin films (a) solution preparation (b) film preparation.

3.2. Film Preparation

3.2.1. Substrate Preparation

All of the BTS-BCT thin films were produced on (111)-Pt/Ti/SiO_2/Si-(100) (INOSTEK - South Korea) substrates by sol-gel method, spin coating. The selection of this substrate was mainly due to thermal expansion coefficient (thermal expansion of top layer Pt is $8.8x10^{-6}K^{-1}$ [85]) and low misfit (2%) between the substrate and thin film. Moreover platinum top layer is proper for high temperature heat treatments. The diffusion between top layer and the film is very limited. Also the conductivity of platinum provides the substrate act as bottom electrode for piezoelectric applications. The substrates are available as 4 inch diameter round discs. So in order to have proper dimensions for usage, the substrates were cut in square shape (1.5 cm x 1.5 cm) in GÜNAM at METU. The substrates may contain contamination even necessary precautions are taken. Because of contamination, before applying the first coating, the substrates were cleaned by ultrasonic alcohol procedure. In ultrasonic bath, rinsing of the substrates was done in acetone to remove any contamination, organics mainly. Later on, rinsing again but this time rinsing in ethanol was done to clean the wafer from acetone and other contamination if any exists. This procedure is finalized in clean room, by drying the substrates under high pressure nitrogen gas.

Table 3.1 Specifications of (111)-Pt/Ti/SiO2/Si-(100) substrate

Pt Layer (Top)	
Fabrication Technique	DC Magnetron Sputtering
Thick. (nm)	150
Oriented	111
Ti Layer	
Fabrication Technique	DC Magnetron Sputtering
Thick. (nm)	10
SiO_2 Layer	
Fabrication Technique	Thermal Oxidation
Thick. (nm)	3000
Si Wafer	
Fabrication Technique	CZ (Prime)
Thick. (μm)	525
Oriented	100

3.2.2. Spin Coating Step

Firsty, the final solution was kept in ultrasonic bath for 15 min every time before coating. Chemat Technology spin coating system was used as spin coater. The substrates were ensured to stay on coater by using double sided tapes due to high rotation speed. The layers thicknesses rely on solution viscosity and rotating speed of the coating system. For best practice, proper speed was selected as 2250 rpm for 30 s. In this step, most of acetic acid and water remove from the surface due to high rotation speed. The thickness of the films was selected as 500 nm. The reason for this selection was to use optimum thickness for electrical properties. If the films were lower than ~400 nm dielectric breakdown happens even in low voltages. Additionally the film is randomly oriented in situation of thick films. So 500 nm film thicknesses was enough for both prevention of dielectric breakdown if voltage no higher than 10V is applied, and also good for growing films with orientation. For desired thickness of 500 nm, multiple (thirteen layers) spin coating-pyrolysis process was applied before sintering the thin films.

3.2.3. Heat Treatment of BTS-BCT Thin Films

Firstly, BTS-BCT thin films are heat treated 15 min with drying at ~200 °C. Remaining chemicals from spin-coating process, except 2-methoxyethanol were removed in drying step. As organics are removed from the coating, inorganic network grows. So, the next step is pre-sintering of the films at 500°C for 15 min. For the desired thin films with thickness of 500 nm, this drying and pre-sintering processes were applied to thin films for thirteen times. At the end, the thin films with amorphous structure were converted to crystalline perovskite structure by sintering process. The different temperatures were selected 700°C, 750°C, 800°C and 850°C according to thermal analysis and temperatures more than 850°C are not proper for platinized silicon substrates. The thin films were heated in the furnace with 10°C/min and kept in sintering temperatures 1 h. The sintering time was kept constant because the sintering times do not affect $BaTiO_3$-based materials microstructures. The sintered thin films were cooled by furnace cooling approach. All of the heat treatments were done in Protherm (PC442) furnace.

3.3. BTS-BCT Thin Film Characterization

3.3.1. Structural and Morphological Analysis

The elemental and phase analysis of the BTS-BCT thin films, XRD analyses were conducted by using Rigaku D/MAX 2200/PC X-Ray Diffractometer between 20° - 60° (2θ) with Cu (Kα) radiation. The coating thickness and morphologies of cross-section and surface of the films were examined by using FEI Nova Nano SEM 430 Field Emission Scanning Electron Microscope. Both of the systems used in analysis belong to METU.

3.3.2. Electrical Properties Measurements

In order to determine dielectric constants and tangent loss of BTS-BCT thin films, capacitance-frequency measurements were conducted by using Agilent 4294A Impedance Analyzer between frequency ranges of 100 kHz-1000 kHz. The Analyzer had the oscillation voltage of 0.05 V at RT. Results for ferroelectric property of BTS-BCT thin films were studied by Radiant Ferroelectric Tester LC (Radiant Technologies, Inc.) . 1, 3, 5, 10 V were applied to the films. Both for dielectric and ferroelectric measurements, the contact between the thin films and measurement systems were provided by Mercury Probe Model 802B-200. Usage of same probe helps to obtain more reliable results. The contact area for this type of probe is 0.00454 cm^2.

3.3.3. Thermal Analysis

Thermal Analysis was done in the Central Laboratory of METU. The Differential Thermal Analysis (DTA) and the Thermogravimetry Analysis (TG) were conducted by Simultaneous Thermogravimetric Analyzer and Differential Thermal Analyzer. By this analysis, important stages where dramatic change in weight and heat changes occur during heat treatment process of the films were observed. So, the data related drying, pyrolysis and annealing temperatures and reactions were obtained.

In order to prepare necessary powders for thermal analysis, the solvent was kept in an opened vessel for 5 h at 100°C temperature.

3.3.4. Viscosity Measurements

The viscosity of the final solution that will be used in spin coating was determined in Thermal Analysis Instruments ARES Rheometer unit in Central Laboratory at Middle East Technical University between shear rates of 10 – 1000 s^{-1}.

CHAPTER 4

RESULTS AND DISCUSSION

This thesis study was done in order to fabricate $BaTiO_3$ based lead-free alternative $Ba(Ti_{0.88}Sn_{0.12})O_3$-$0.3(Ba_{0.7}Ca_{0.3})TiO_3$ (BTS-BCT) thin films by using sol-gel method that should be used in ferroelectric, dielectric and piezoelectric applications. By an aspect of sol-gel method, spin coating made it possible to obtain homogeneous and stock solutions and fabricate crack-free and smooth thin films. $(Ba_{0.91}Ca_{0.09})(Ti_{0.92}Sn_{0.08})O_3$ composition was selected due to its close location to morphotropic phase boundary (MPB) and existence of tricritical point type MPB in BTS-BCT compositions. In order to determine optimum parameters for BTS-BCT thin film fabrication, the samples with 500 nm thickness and sintered 1 h at various sintering temperatures (700°C, 750°C, 800°C, 850°C) were examined. The optimum film thickness 500 nm was selected due to dielectric breakdown problem in thinner films and while higher probability of random orientation of grains and cracks in thicker films those may utterly decrease or vanish electrical properties, respectively. Keeping the molarity relatively low in order to promote oriented grains, using the solution with 0.4 M resulted thirteen multiple layers of coating method to obtain thin films with 500 nm thickness. The thickness of the films was measured by SEM study. The results of analyses and measurements of the samples sintered at different temperatures, indicated 850°C is the optimum sintering temperature. In Table 4.1 experimental of fabricated sample details may be seen.

Table 4.1 Experimental details of samples fabricated

Composition	Sintering Temperature for 1 h	Number of layers coated
$(Ba_{0.91}Ca_{0.09})(Ti_{0.92}Sn_{0.08})O_3$	700°C	13
$(Ba_{0.91}Ca_{0.09})(Ti_{0.92}Sn_{0.08})O_3$	750°C	13
$(Ba_{0.91}Ca_{0.09})(Ti_{0.92}Sn_{0.08})O_3$	800°C	13
$(Ba_{0.91}Ca_{0.09})(Ti_{0.92}Sn_{0.08})O_3$	850°C	13

4.1. Thermal Analysis

Thermal analysis on powders obtained from precipitated solution, were performed to determine critical temperatures and weight losses occurring due to heating. The powders, obtained by keeping the solution at 100°C for 5 h were heated up to 1000°C with a heating rate of 10°C/min and Thermogravimetric and Differential Thermal Analysis were applied on these powders. Regarding the results of analysis, proper temperatures of drying, firing and sintering were decided.

By differential thermal analysis (DTA) curve, exothermic and endothermic reactions were observed while thermogravimetry (TG) curves provided weight losses determination. Both of the approaches resulted in understanding of important stages that BTS-BCT powders are exposed. DTA and TG curves of lead-free $(Ba_{0.91}Ca_{0.09})(Ti_{0.92}Sn_{0.08})O_3$ composition powders are illustrated in Figure 4.1 and Figure 4.2, respectively.

The differential thermal analysis (DTA) curve indicates the endothermic and exothermic reactions which were used to obtain critical stages during heating of the BTS-BCT powders up to 1000°C. Moreover, the thermogravimetry (TG) graph indicated the weight loss. Graphs of TG, DTA and integrated graph of both for $(Ba_{0.91}Ca_{0.09})(Ti_{0.92}Sn_{0.08})O_3$ composition are shown in Figure 4.1, Figure 4.2, and Figure 4.3 respectively.

In Figure 4.2, Thermogravimetry (TG) graph results can be divided into three main weight loss regions. The first region consists of 12% weight loss that the loss has a stable slope until temperatures around 200°C. In this region remaining chemicals from spin-coating step, large amount of the solvent (acetic acid and 2-methoxyethanol) are removed. When 200 °C temperatures are exceeded the weight loss increases dramatically until temperatures around 500°C. In this second weight loss region 26.5% weight loss occurs due to the decomposition of acetates and organic compounds. In third region, between 500-800°C temperatures 9% weight loss occurs. Beyond temperatures higher than 800°C no significant weight loss occurs. In the final region inorganic phase is obtained. In Figure 4.1, there is a sharp decrease in heat flow at 783 °C that indicates the crystallization of the material, perovskite formation. Even though some crystallization may occur at lower temperatures 783°C, the majority of the crystalline grains will form at temperatures beyond 783°C. Hence, the optimum sintering temperature should be higher than 783°C. In order to obtain optimum temperature more detailed study should be done that will be given in following parts.

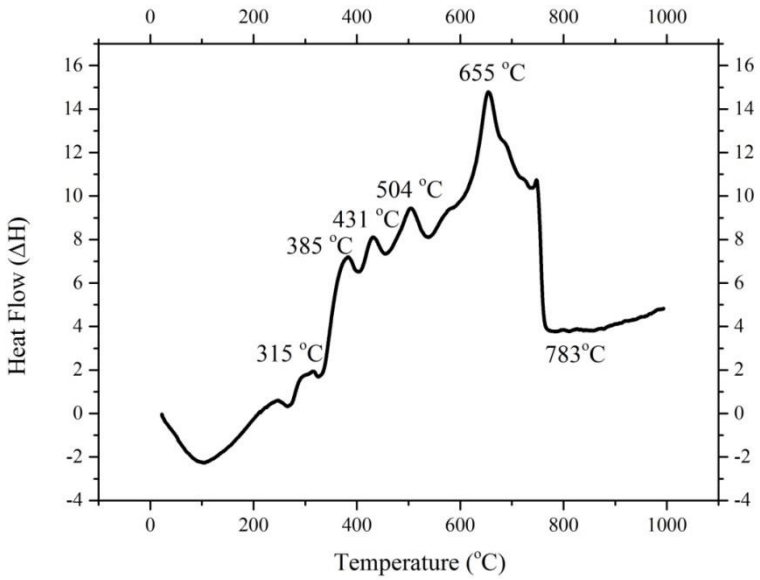

Figure 4.1 DTA graph of $Ba(Ti_{0.88}Sn_{0.12})O_3-0.3(Ba_{0.7}Ca_{0.3})TiO_3$ powders

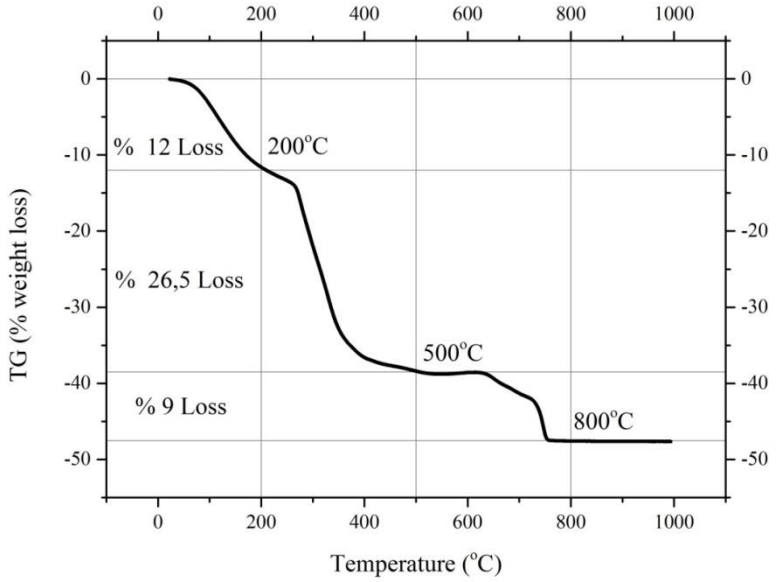

Figure 4.2 TG graph of $Ba(Ti_{0.88}Sn_{0.12})O_3-0.3(Ba_{0.7}Ca_{0.3})TiO_3$ powders

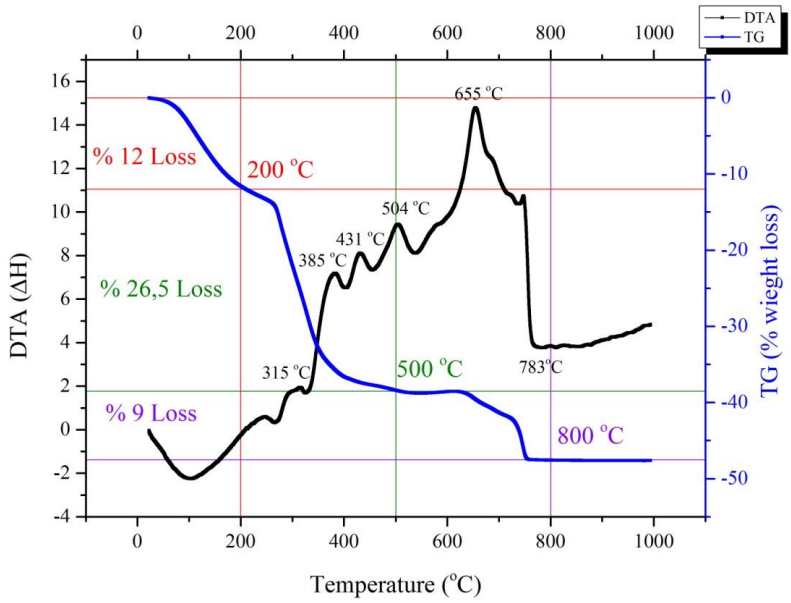

Figure 4.3 Integrated graph of TG and DTA

4.2. Viscosity Measurements of BTS-BCT Solutions

Viscosity measurement was performed in order to be ensured that the solution is homogeneous. The solution homogeneousness is vital for crack-free and smooth film

formation.

The viscosity (Pa.s) – shear rate (1/s) curve prepared for $(Ba_{0.91}Ca_{0.09})(Ti_{0.92}Sn_{0.08})O_3$ thin films can be seen in Figure 4.4. The viscosity of the solution does not change much with variation in the shear rate; this situation states the uniformity of the solution. By equating the output from measurement into simple arithmetic average equation, the average viscosity of the solution is calculated 0.002162 Pa.s.

By power-law index, the solution is Newtonian. Newtonian solutions are uniform and homogenous solutions which the viscosities do not vary much with different shear rates.

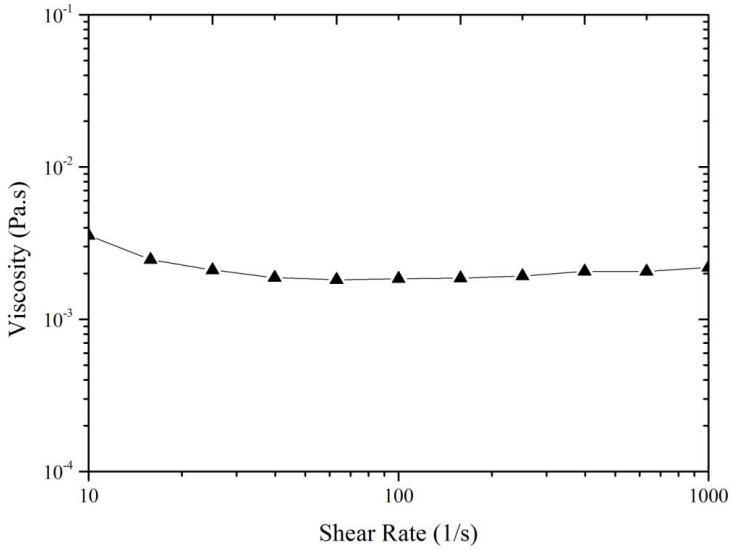

Figure 4.4 Viscosity versus shear rate of $(Ba_{0.91}Ca_{0.09})(Ti_{0.92}Sn_{0.08})O_3$ solution

4.3. Crystalline Film Formation

XRD studies were used in order to determine the existence of perovskite phase. The thicknesses were kept 500 nm. (111)-Pt/Ti/SiO_2/Si-(100) wafers were used. The pyrolysis temperature was kept constant at 500 °C. Effect of the sintering temperatures of 700°C, 750°C, 800°C, 850°C in BTS-BCT thin films were compared and a pyrochlore phase was observed. The sintering time was kept 1 h for all sintering temperatures. $BaTiO_3$ with perovskite structure has a X-ray pattern with

2θ= 22° (100), 33° (110), 38° (111), 46° (200), 52° (210) and 57° (211) peaks between 20°- 60°.

In Figure 4.5 virgin, uncoated condition of substrate is shown. The spectrum of the substrates helps to determine which peaks belong to desired structure, substrate or pyrochlore. The main peak is at 2θ=40.25° which is Pt (111) with JCPDS file number of 88-2343. Moreover, at 2θ=36.16° Pt (111) has additional peak due to CuK_{β} diffraction. Generally using monochromatic filter should eliminate all other types of Cu radiations but CuK_{α} radiation. Even though the elimination due to monochromatic filter, this peak has been observed in some studies which platinized silicon substrates are used [86]. Addition to Pt peaks, Si peak at 2θ=33.12° with JCPDS file number of 17-0901 was observed. It should be noted importantly that the relatively weak peaks of Si and Pt which belong to substrate are not observed in every X-ray diffractogram.

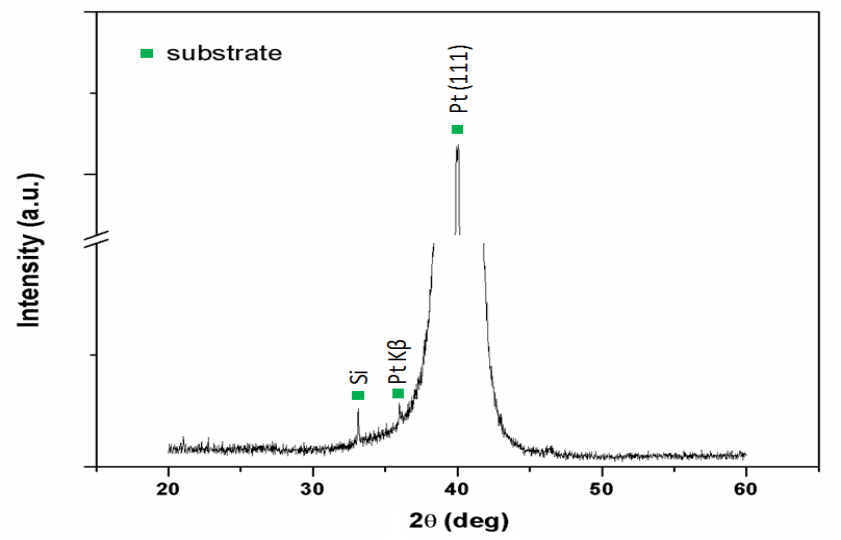

Figure 4.5 X-ray diffractogram of substrate [76]

In Figure 4.6, pure perovskite can be observed. BTS-BCT thin film has typical polycrystalline microstructure of perovskite $BaTiO_3$. The strongest peak belongs to (110) peak in typical $BaTiO_3$. In the diffractogram of the thin film sintered at 700 °C Pt (111) peak overlaps the peak of (111) perovskite. In Figure 4.7, BTS-BCT sample sintered at 750 °C is has pure perovskite phase similar with the sample sintered at

700 °C. (111) peak of perovskite structure has grazed slightly from (111) peak of Pt. Addition to (111) Pt peak, peaks from PtK_{β} and Si can be noticed.

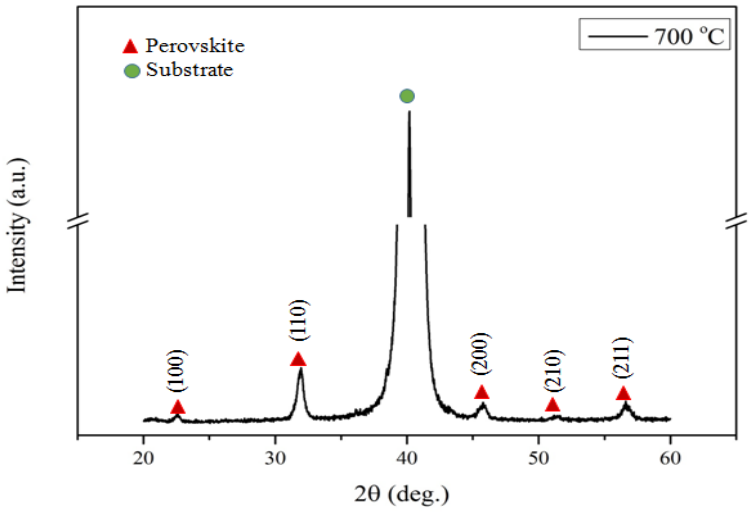

Figure 4.6 X-ray diffractogram of $(Ba_{0.91}Ca_{0.09})(Ti_{0.92}Sn_{0.08})O_3$ thin film sintered at 700°C

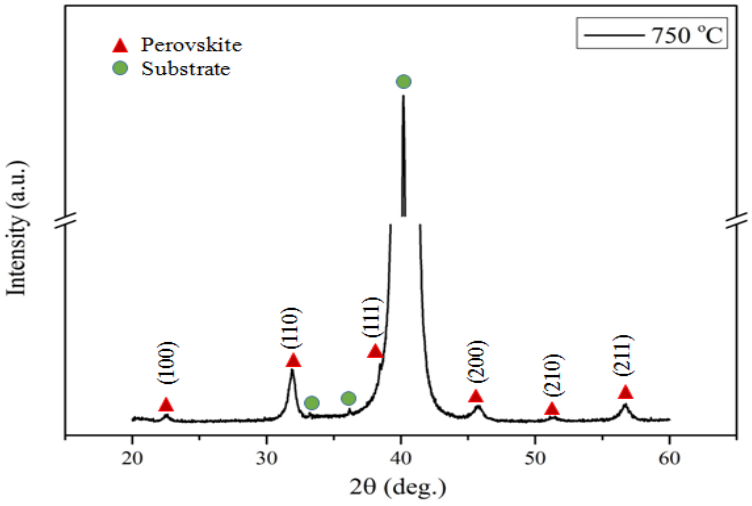

Figure 4.7 X-ray diffractogram of $(Ba_{0.91}Ca_{0.09})(Ti_{0.92}Sn_{0.08})O_3$ thin film sintered at 750°C

In Figure 4.8 and 4.9 the (111) peak of perovskite, which is the preferential orientation can be clearly seen. As explained in previous chapters, the preferential

orientation of (111) promotes electrical properties. In these samples sintered at 800°C and 850°C the diffractograms show polycrystalline structure but different than the samples sintered at lower temperatures, at 800°C and 850°C the most desired peak of tetragonal structure which shows the oriented growth of grains, the sharp peak of (111) perovskite can be observed clearly. Even though the (111) peaks of samples sintered at 800°C and 850°C become visible due to higher intensities, it can not be suggested that the oriented growth has been completely achieved, actually the sharp and strong peaks of (111) perovskite indicate only the improved growth of grains in (111) direction. On the other hand, in addition to having perovskite phase, pyrochlore phase appears, which is most probably Ti_2O_3 at $2\theta = 33°$ with JCPDS file number 76-0145. The pyrochlore is stable for 800°C and 850°C temperatures.

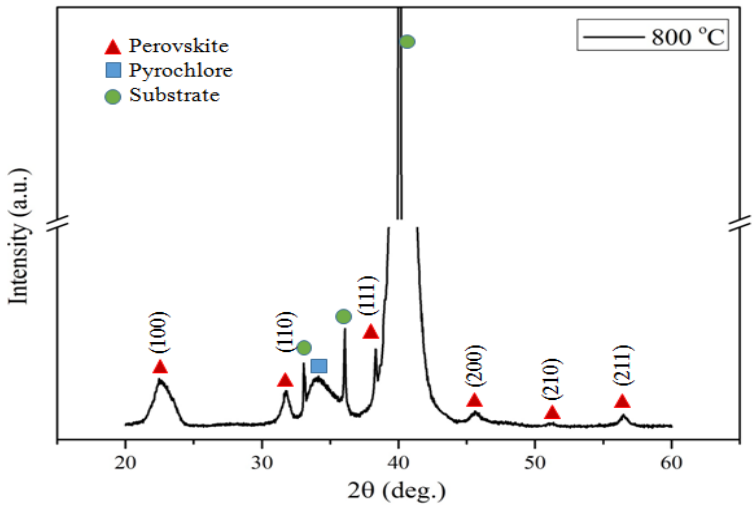

Figure 4.8 X-ray diffractogram of $(Ba_{0.91}Ca_{0.09})(Ti_{0.92}Sn_{0.08})O_3$ thin film sintered at 800°C

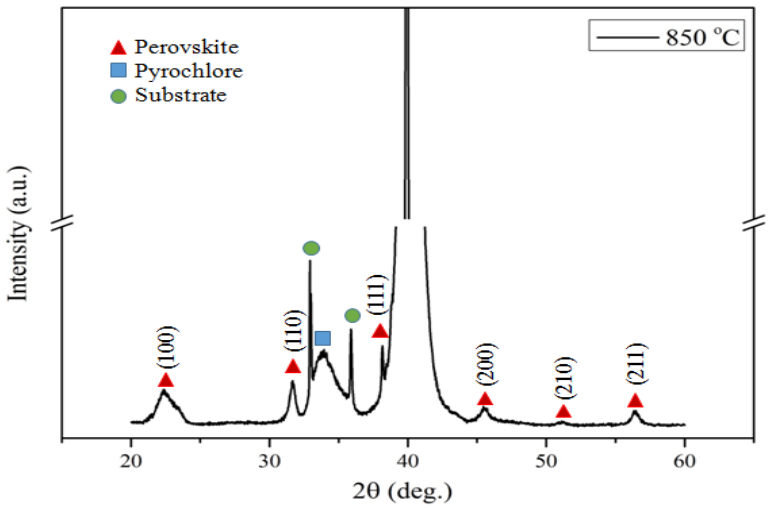

Figure 4.9 X-ray diffractogram of $(Ba_{0.91}Ca_{0.09})(Ti_{0.92}Sn_{0.08})O_3$ thin film sintered at 850°C

As a result of diffractograms, this composition, as a derivation of $BaTiO_3$ based compositions also fail to exhibit well oriented growth. The homogeneous nucleation cause small grains and prevents columnar growth. Even though increase in (111) peak indicates an increase in (111) oriented grains, the polycrystalline structure of BTS-BCT thin films as a $BaTiO_3$ based compositions, can be clearly seen. The comparison between the samples sintered at different temperatures is shown in Figure 4.10.

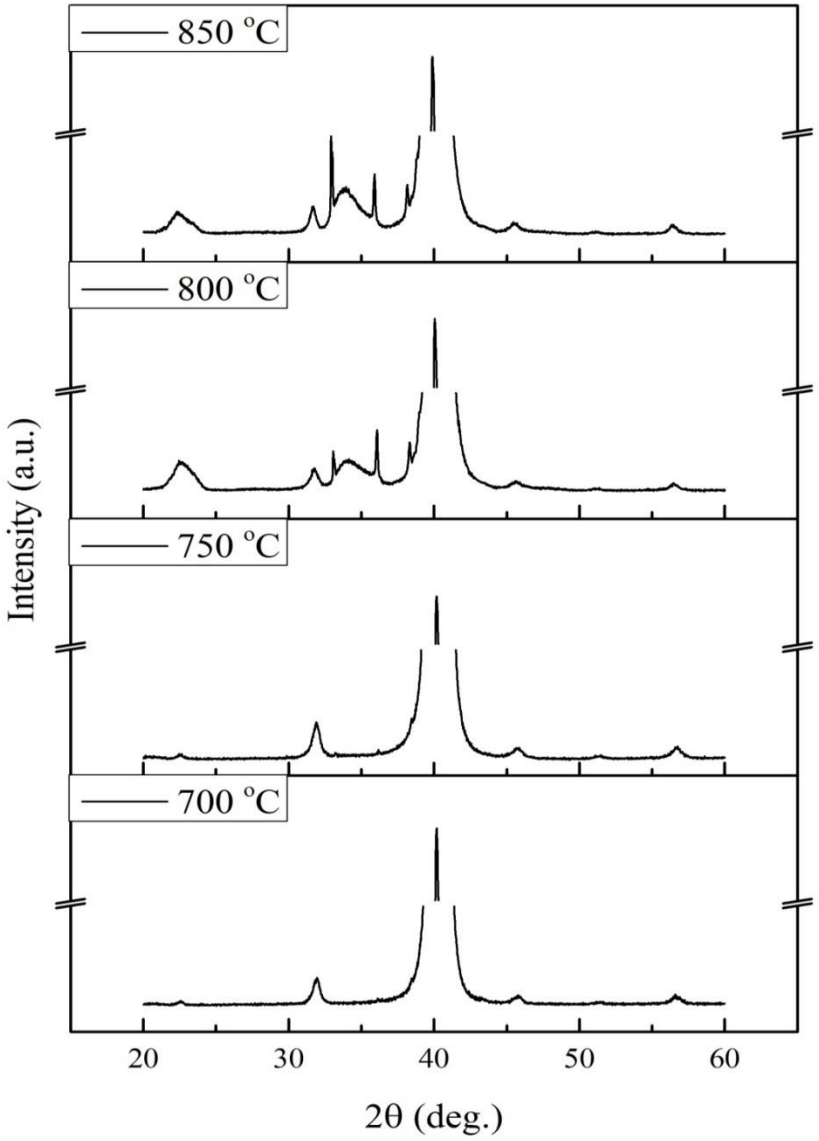

Figure 4.10 X-Ray diffraction patterns samples for different sintering temperatures

4.4. Morphology of BTS-BCT Thin Films

The surface morphologies were examined and thin film thicknesses were obtained by using Field Emission Scanning Electron Microscope (FESEM). To achieve 500 nm thin film thickness, thirteen layers were produced. The molarity of the solutions was kept constant at 0.4 M. The spin coating process was determined as 2250 rpm coating for 30 s.

The thermal mismatch of the substrate and BTS-BCT thin films and conversion of the gel into dense structure generate stresses which may cause crack formation. The stress generated by thermal mismatch may cause cracks between the thin film and the substrate, while stress generated by conversion of gel into dense structure may cause cracks on the surface of the thin films which can utterly vanish or diminish ferroelectric or dielectric response. In order ensure that the thin films are crack free, the surface morphology was examined in lower magnifications. Figure 4.11 to 4.13 illustrate some examples of the surface morphologies which belong to samples sintered at 850°C and the photographs of samples were obtained by 2500X, 1200X, 600X magnification.

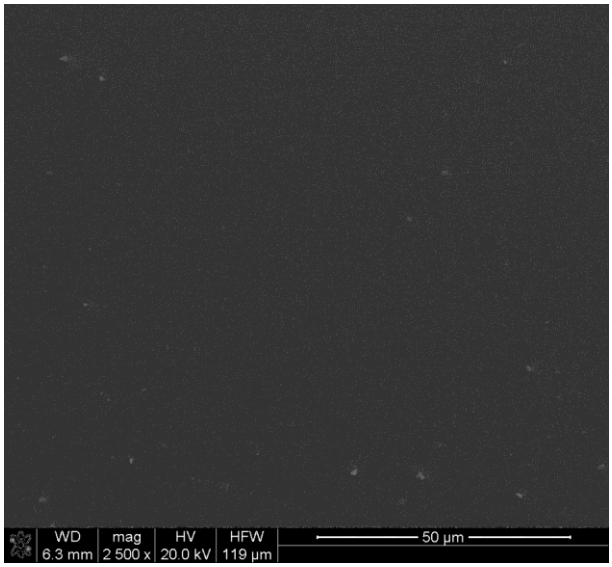

Figure 4.11 FESEM image of BTS-BCT sample sintered at 850°C at 2500X magnification

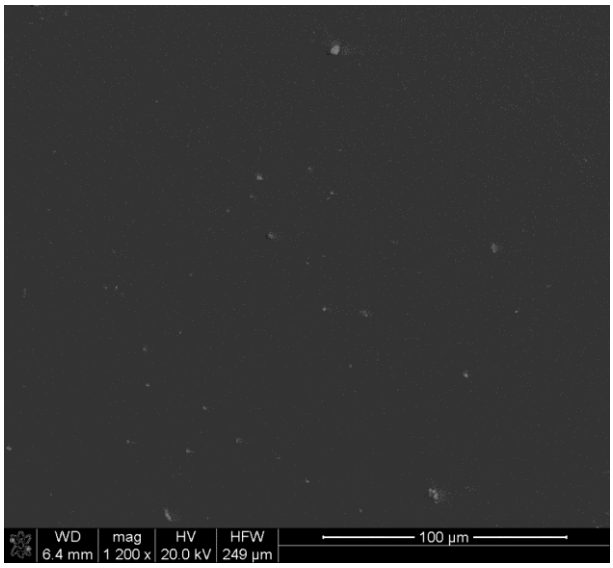

Figure 4.12 FESEM image of BTS-BCT sample sintered at 850°C at 1200X magnification

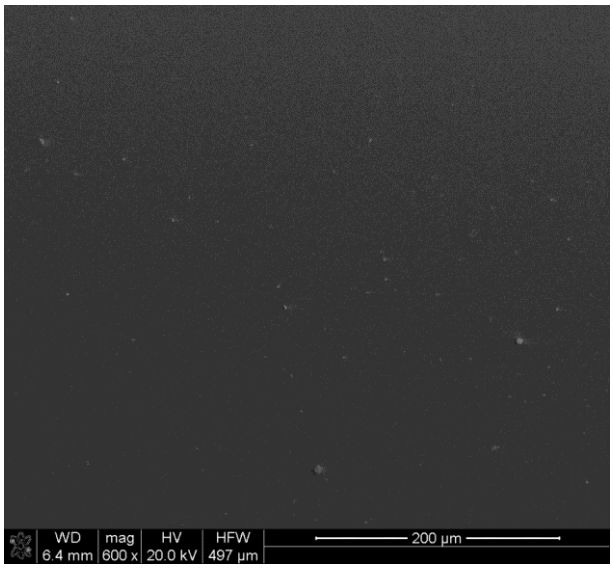

Figure 4.13 FESEM image of BTS-BCT sample sintered at 850°C at 600X magnification

From Figure 4.14 to 4.21, SEM images of cross section and surface morphology of the thin films sintered at different temperatures are shown. Figure 4.14 and Figure 4.15 clearly reveal the porous structure of BTS-BCT thin films sintered at 700°C. Figure 4.14 illustrates the well sticking behavior of the thin films within the thin

films. The surface roughness is high. In Figure 4.15 the thin film shows a small grained structure with grain size as small as 20-30 nm.

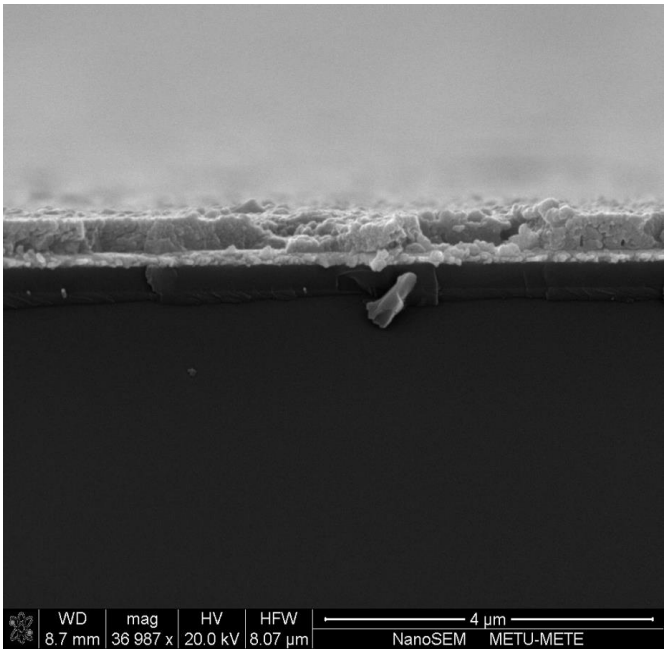

Figure 4.14 FESEM cross-sectional image of BTS-BCT thin film sintered at 700°C

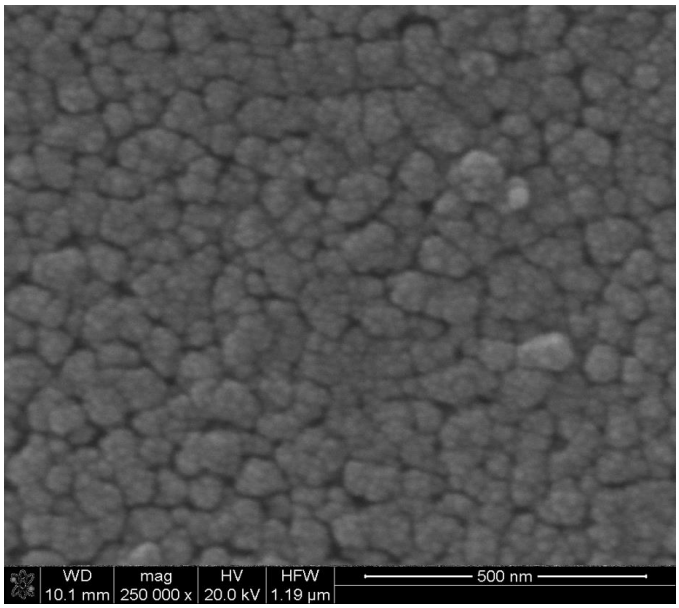

Figure 4.15 FESEM image of BTS-BCT sample sintered at 700°C

At 750°C, some of the small grains begin to agglomerate that leads to formation of larger grain structure while other grains have obvious grain boundaries. Pores at different points can be observed easily. The microstructures which have agglomerate

like structure have the pronounced edges in the secondary electron image that likely indicates the variations in thickness, indicating the potential that electrically weak points might form due to uncontrolled crystallization [87].

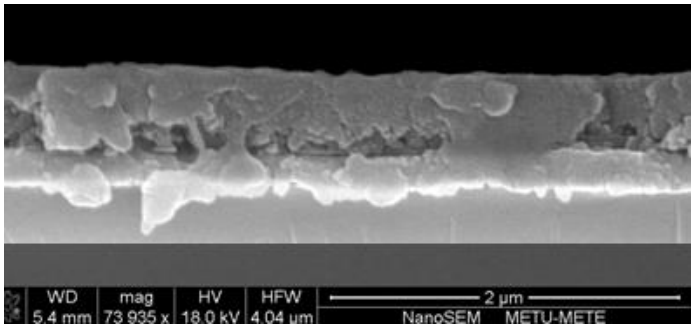

Figure 4.16 FESEM cross-sectional image of BTS-BCT thin film sintered at 750°C

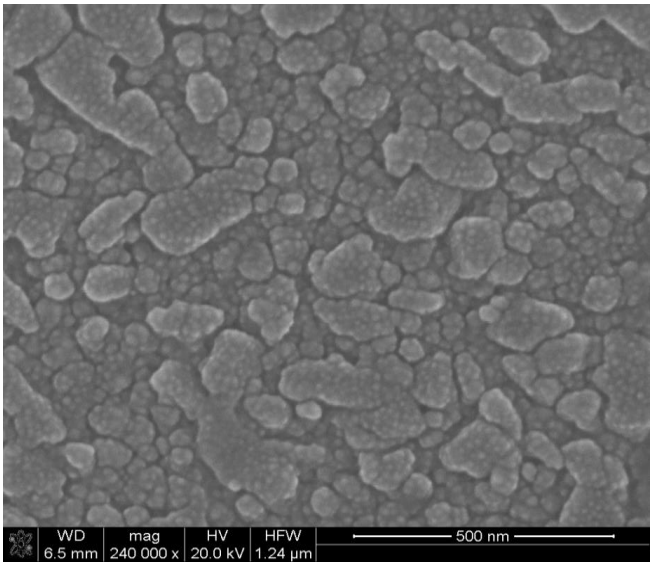

Figure 4.17 FESEM image of BTS-BCT sample sintered at 750°C

As Figure 4.18 and 4.21 indicate, the thin films fabricated at the temperatures of 800°C and 850°C have more dense structure than the thin film fabricated at lower temperatures. However the surface of the films is rough. Additionally, Figure 4.19 and Figure 4.21 show that the thin film microstructures look like agglomerates of small grains. Similar to sample sintered at 750°C, samples sintered at 800°C and 850°C have the pronounced edges and areas in the secondary electron image which may indicate the thickness variations [87]. For the sample sintered at 850°C these

pronunciations are lesser than the sample sintered at 800°C. Nevertheless the films were crack and hole free. The microstructure is inhomogeneous that the both microstructures like agglomerates with larger grains and small grains with different grain sizes are present. The grains are randomly oriented.

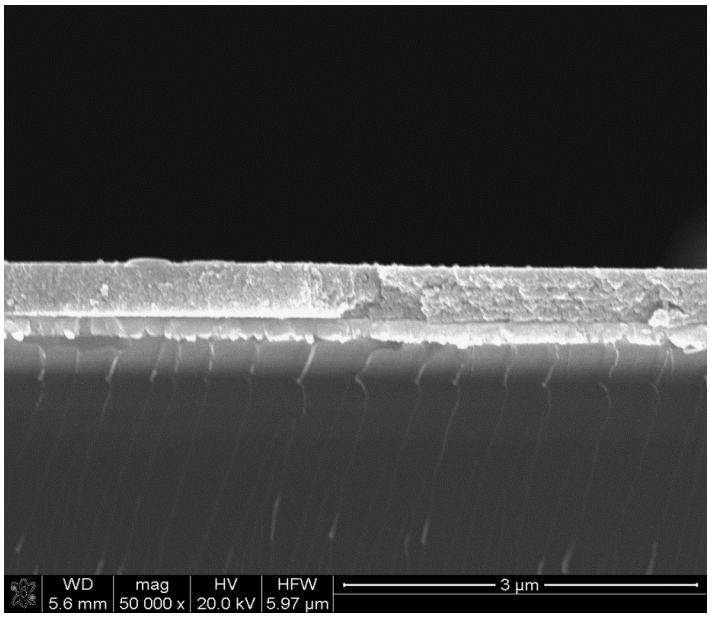

Figure 4.18 FESEM cross-sectional image of BTS-BCT thin film sintered at 800°C

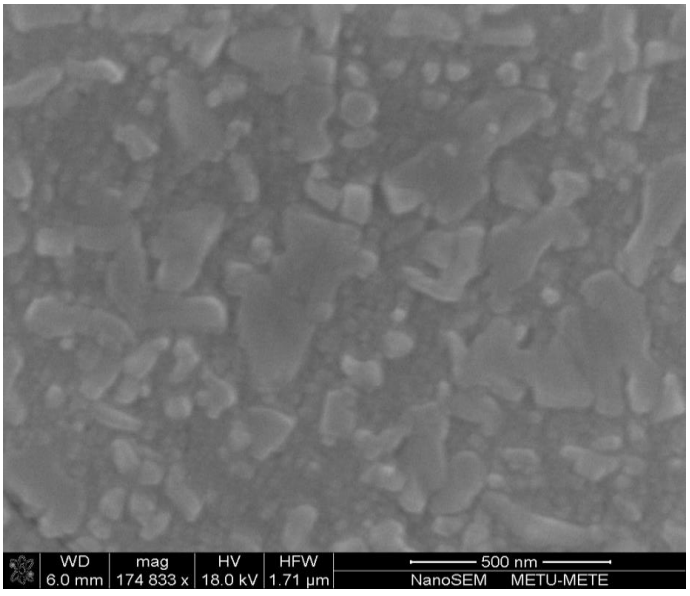

Figure 4.19 FESEM image of BTS-BCT sample sintered at 800°C

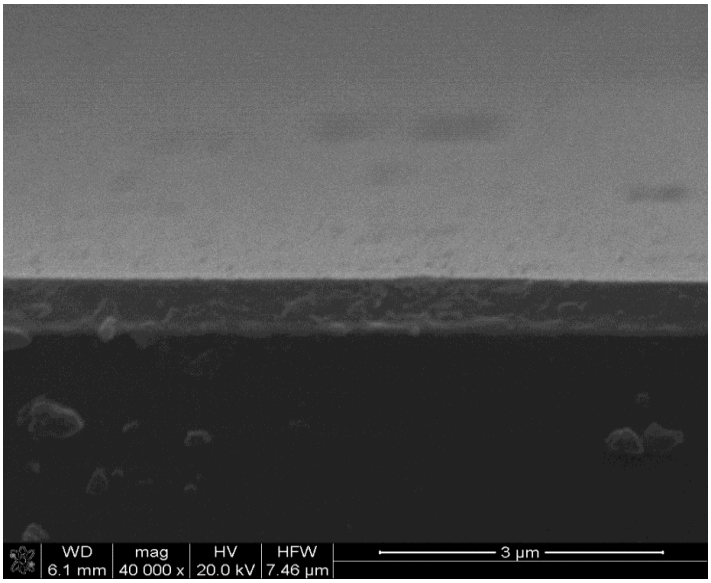

Figure 4.20 FESEM cross-sectional image of BTS-BCT thin film sintered at 850°C

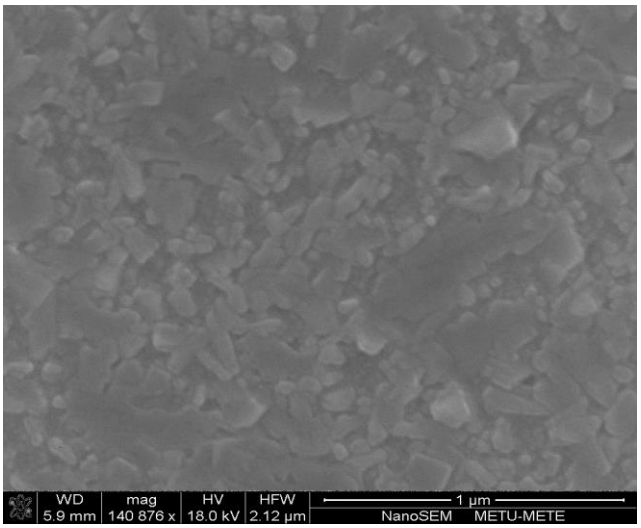

Figure 4.21 FESEM image of BTS-BCT sample sintered at 850°C

To understand the microstructure difference between PZT and $BaTiO_3$ based thin films, the main growth mechanism should be explained. In PZT thin films, generally columnar structure is obtained. This is due to the nucleation of PZT perovskite phase at the interface between the thin film and substrate. So, PZT grains grow from the

interface towards the surface. As the grains grow, the pyrochlore phases within the film are consumed in columnar, large PZT grains. In addition to this factor, the low sintering temperatures of PZT (around 600 °C) also favor heterogeneous nucleation. Due to lower driving force, the pyrochlore phases can not exceed the critical nucleation size. So that, once the pyrochlore phases promote heterogeneous nucleation at the interface between substrate and film, pyrochlore phases are consumed in PZT growing grains within the bulk. So PZT thin films have columnar structure and if the substrates have a favorable orientation such as (111)-Pt/Ti/SiO_2/Si-(100) then the highly oriented columnar grains will be observed in SEM images and the X-ray diffractogram [88]. On the other hand, in $BaTiO_3$ based compositions homogeneous nucleation is dominant. The nucleation of perovskite phase occurs homogeneously within the bulk of the thin film. Relatively high sintering temperatures (generally around 800°C) of $BaTiO_3$ based composition provide large driving forces which promote homogeneous nucleation for perovskite $BaTiO_3$ and pyrochlores. Provided by higher driving force, pyrochlores can exceed the critical nucleation energy. The intermediate phases overcome critical sizes and continue to grow and act as growth point within the bulk. So, homogeneous nucleation within amorphous matrix of the film and heterogeneous nucleation at the electrode interface occur simultaneously. This theory explains the microstructural properties of BTS-BCT thin films [89]. Additionally, in the study of Schwartz, that Pt substrates were used for thin film fabrication, the different nucleation and growth mechanisms of PZT and BT have been observed clearly [90]. In Figure 4.22, the PZT films nucleated at Pt electrode are single grain thick with a columnar structure, while BT films have nucleation at the interface and within the bulk of the film and porous structure.

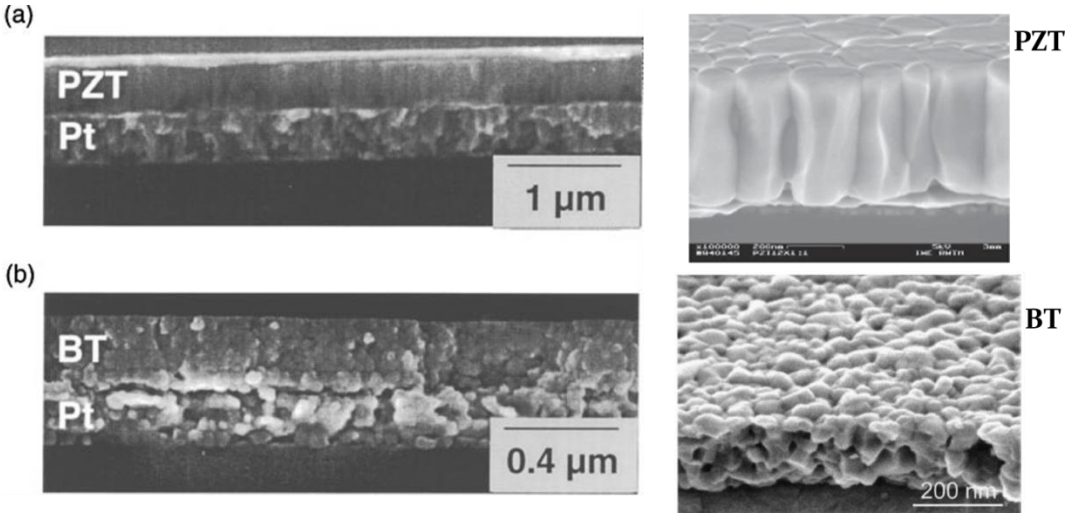

Figure 4.22 (a) The PZT film exhibits nucleation only at the Pt electrode interface. PZT films usually have columnar structure and are only a single grain thick; (b) The BT film exhibits nucleation both at electrode interface and within the film. BT films are porous [89-91]

The theory of different nucleation and growth mechanism of PZT and BT based compositions are illustrated in Figure 4.23.

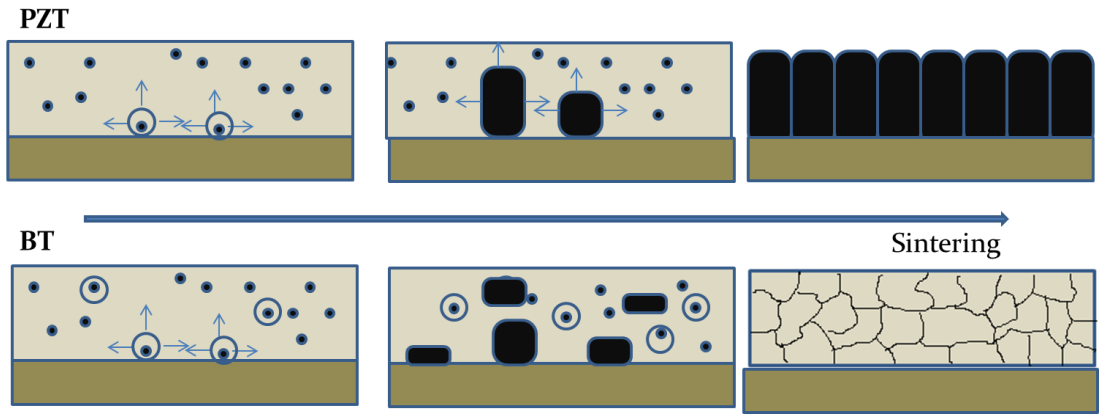

Figure 4.23 In PZT composition, intermediate phases act as nuclei at the interface but within the film, they combine to the columnar structure during the sintering stage. In BT based compositions, the intermediate phases overcome the critical sizes and continue to grow and act as growth points within the bulk. Both homogeneous nucleation within the bulk of the film and heterogeneous nucleation at the electrode interface occur simultaneously.

The porous structure of BTS-BCT thin films is also related with Sn content. In a study that investigates $BaSn_xTi_{(1-x)}O_3$, tin addition induces an obvious disturbance in microstructure refinement, which clearly affects the densification, contributing to the appearance of a certain amount of intergranular porosity and decrease in average grain size [92]. Additionally, in the study with composition $(Ba_{0.90}Ca_{0.10})(Ti_{1-x}Sn_x)O_3$ the microstructure is inhomogeneous due to tin content at x=0.08, while at x=0.06 the microstructure becomes significantly homogeneous [17].

4.5. Dielectric Properties of BTS-BCT Thin Films

The dielectric properties of BTS-BCT thin films were determined by capacitance-frequency measurements by using Agilent 4294A Impedance Analyzer between frequency ranges of 100 kHz-1000 kHz with the oscillation voltage of 0.05 V at RT. The dielectric properties such as capacitance (C), permittivity (ϵ_r), and tangent loss ($\tan\delta$) were obtained and the effect of sintering temperatures in 1 h sintered thin films with 500 nm thickness were examined in these measurements.

A stable capacitor does not vary much from direct current to microwave frequencies and it is essential to select a proper capacitor for working frequencies [93]. During switching, the orientation action of domains needs time due to movement of dipoles. There exists a characteristic time for the adjustment of polarization orientation. This characteristic time is called as relaxation time. Consequently very high frequencies result in no response in polarization orientation to adapt the alternating electric field, the polarization orientation inability to stay in direction of applied field. In this manner, exceeding the characteristic frequency causes reduce in polarization of the material [94].

Low dielectric loss is desired for efficiency and avoiding the over-heating of electronic materials. The dielectric loss is caused by two factors, resistive loss and relaxation loss. First factor is caused by the fact that, mobile charges dissipate energy while in relaxation loss, relaxation of dipoles dissipate energy. Consequently, relaxation loss mechanism is dominant if there are a few charges in the films. Resistive loss is directly related with leakage current, if leakage current is high,

resistive loss is also high. On the other hand, in dielectric materials with high dielectric constants, an increase in dielectric loss is mostly caused by relaxation loss. High permittivity results in increased dissipation during relaxation [95].

Capacitance-frequency measurement of thin film sintered at 800^{o}C has been given in Figure 4.24. As explained before, dielectric constant of the thin film, ϵ_r can be calculated by using the following equation,

$$C = \frac{\epsilon_r \times \epsilon_o \times A}{d} \qquad \text{Eq. [2.5]}$$

where C is capacitance, ϵ_o is 8.85x10^{-12} F/m, d is 500 nm, A represents are of probe 0.00454cm^2. Thus, dielectric constant – frequency curve was obtained.

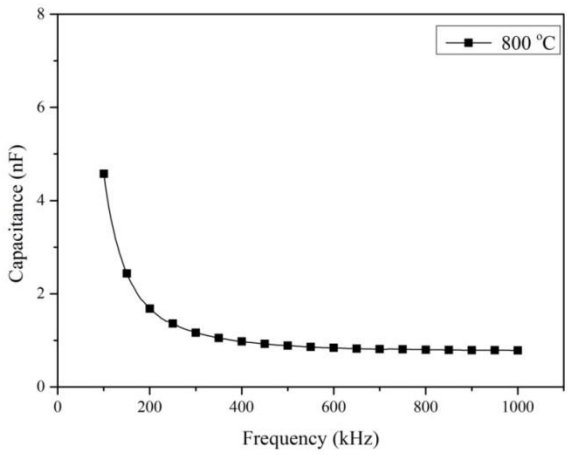

Figure 4.24 Capacitance-Frequency curves of BTS-BCT thin films sintered at 800°C

Figures 4.25, 4.26 show permittivity and tangent loss curves of BTS-BCT thin film sintered at 800°C, respectively. For a randomly selected frequency, at 400 kHz capacitance of BTS-BCT thin film that is sintered at 800°C is 0.97 yields dielectric constant of 121.1 by using Equation 2.5. The tangent loss at this frequency is 6.48 %.

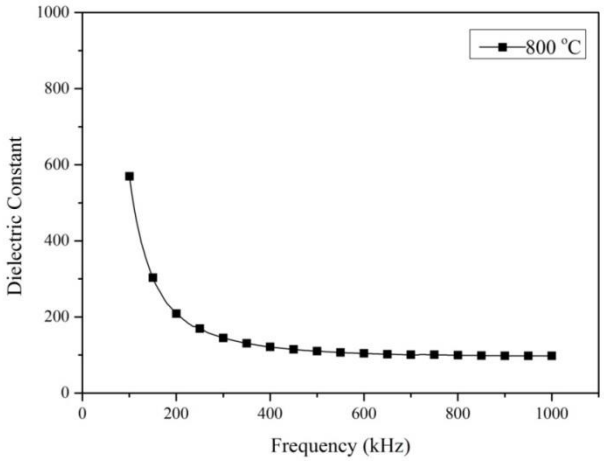

Figure 4.25 Dielectric Constant-Frequency curves of BTS-BCT thin films sintered at 800°C

The Agilent 4294A Impedance Analyzer provided dielectric loss as a direct output in the measurements. The results for dielectric loss shown in Figure 4.26 is compatible with Debye formula, at lower frequencies tan δ is inversely proportional to frequency.

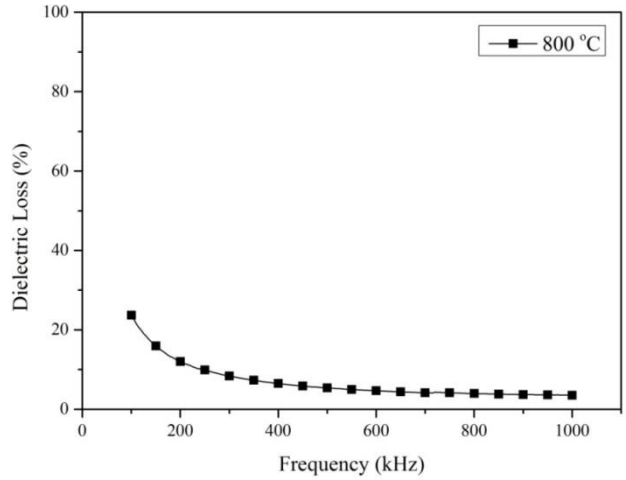

Figure 4.26 Dielectric loss-Frequency curves of BTS-BCT thin films sintered at 800°C

So, after illustrating the results separately for BTS-BCT thin film sintered at 800°C, dielectric properties of samples sintered at different temperatures can be listed in Table 4.2.

Table 4.2 Dielectric properties of the samples up to 1000 kHz frequency

		Frequency (kHz)				
Sintering Temperature		200 kHz	400 kHz	600 kHz	800 kHz	1000 kHz
700°C	Capacitance (nF)	0.45	0.40	0.39	0.39	0.39
	Dielectric Loss (%)	3.47	1.97	1.41	1.13	0.97
	Dielectric Constant (K)	55.5	49.65	48.4	48.1	48.2
750°C	Capacitance (nF)	0.77	0.61	0.57	0.56	0.56
	Dielectric Loss (%)	5.19	3.27	2.38	1.91	1.64
	Dielectric Constant (K)	96.8	75.88	71.0	69.5	69.4
800°C	Capacitance (nF)	1.68	0.97	0.84	0.80	0.78
	Dielectric Loss (%)	12.01	6.48	4.67	3.94	3.53
	Dielectric Constant (K)	209.0	121.1	104.1	99.3	97.6
850°C	Capacitance (nF)	2.24	1.11	0.91	0.84	0.82
	Dielectric Loss (%)	14.84	7.78	5.46	4.36	3.77
	Dielectric Constant (K)	279.4	139.1	113.4	105.1	102.2

For BTS-BCT thin film sintered at 700°C and 750°C, the relation permittivity and dielectric loss as a function of frequency can be seen in Figure 4.27 and 4.28, respectively. The BTS-BCT thin film sintered at 700°C has the lowest dielectric constant (around 50) mainly caused by limited polarization density due to small grain structure. Additionally, the grain boundaries act as path ways for conduction. Moreover, the porous structure of the material reduces the permittivity, additionally the surface porosity acts as moisture source which causes ionic conduction [96]. The dielectric loss is low mainly due to having low permittivity. Even this thin film exhibits the lowest dielectric constant it has the most stable dielectric constant curve with respect to frequencies.

The BTS-BCT thin film sintered at 750°C has higher dielectric constant than the thin film sintered at 700°C. The dielectric constant of this sample does not change much while dielectric loss varies in frequency range between 100-400 kHz.

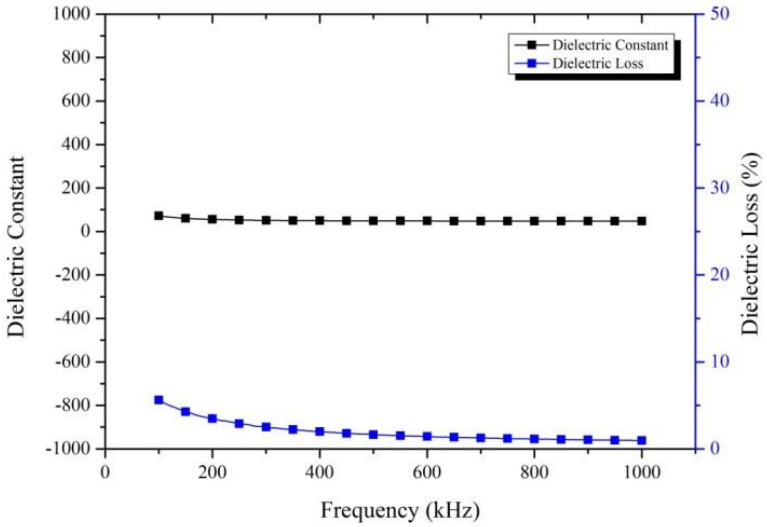

Figure 4.27 Dielectric Constant-Dielectric Loss-Frequency curves of BTS-BCT thin films sintered at 700°C

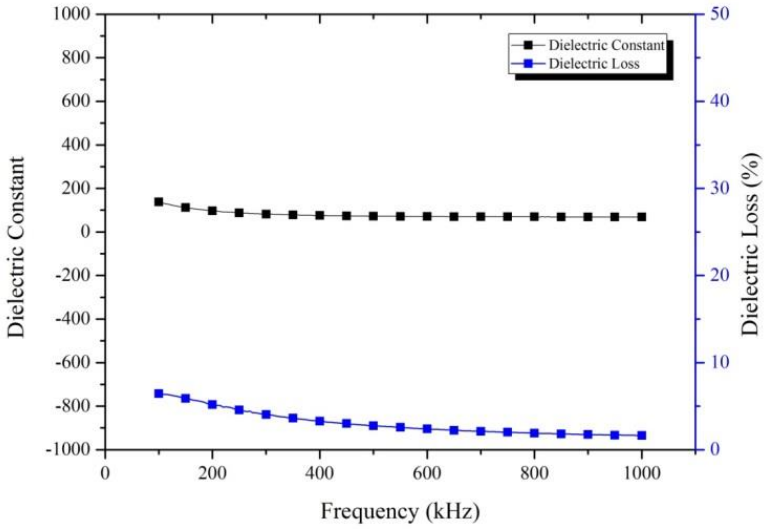

Figure 4.28 Dielectric Constant-Dielectric Loss-Frequency curves of BTS-BCT thin films sintered at 750°C

Compared to thin films sintered at 700°C and 750°C, the thin films sintered at higher temperatures of 800°C and 850°C exhibit higher dielectric constant and dielectric loss (Figure 4.29 and Figure 4.30). Having larger grains promotes higher dielectric constants of samples sintered at 800°C and 850°C because of larger polarization

density existence in larger grains [97]. Larger grains also results in lesser grain boundary density which results in decreased amount of possible, favorable sites for conduction. As mentioned in this section, the dielectric materials with high dielectric constants exhibit high dielectric loss that is relaxation loss. High permittivity results in increased dissipation during relaxation. So, for instance in Figure 4.30 at 100 kHz, the high dielectric loss (29.3%) of sample with high dielectric constant (843) sintered at 850°C should be related with this reason.

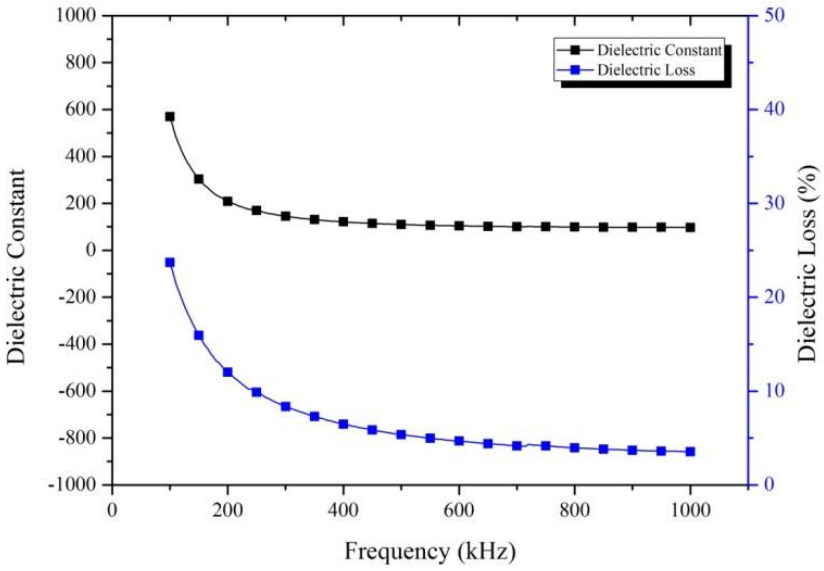

Figure 4.29 Dielectric Constant-Dielectric Loss-Frequency curves of BTS-BCT thin films sintered at 800°C

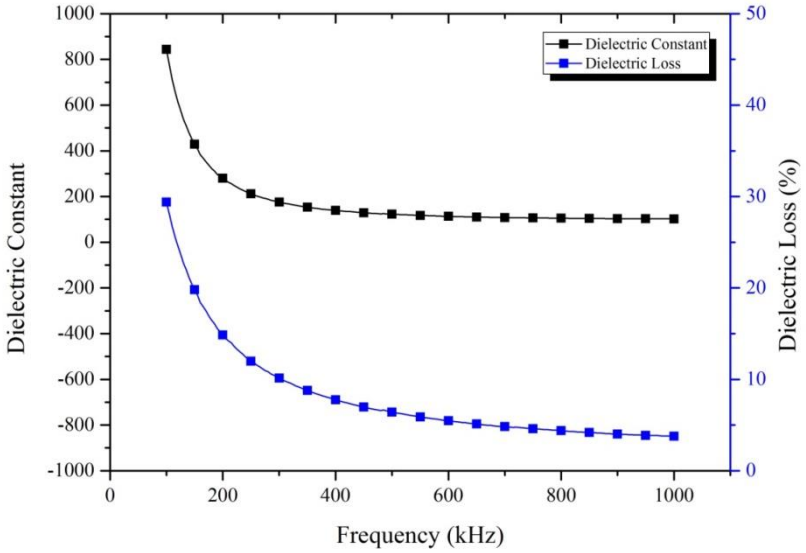

Figure 4.30 Dielectric Constant-Dielectric Loss-Frequency curves of BTS-BCT thin films sintered at 850°C

Hence the capacitance, dielectric measurements for all of the samples will be shown together for better comparison in Figures 4.31 – 4.33.

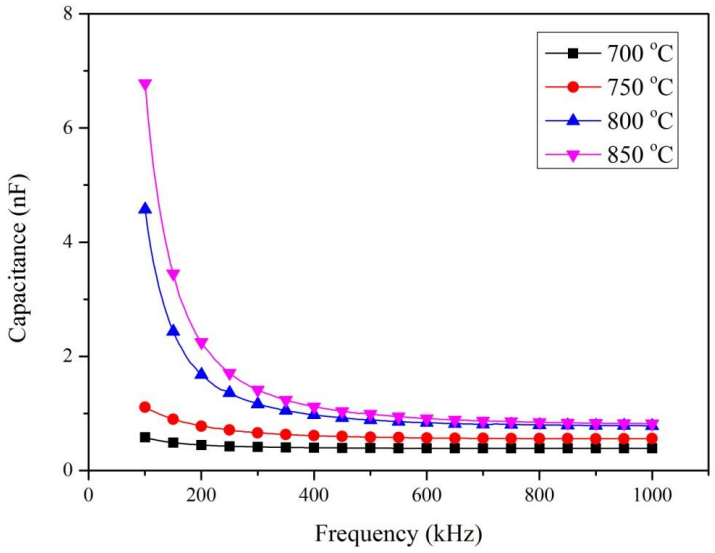

Figure 4.31 Capacitance-Frequency curves of BTS-BCT thin films sintered at different temperatures

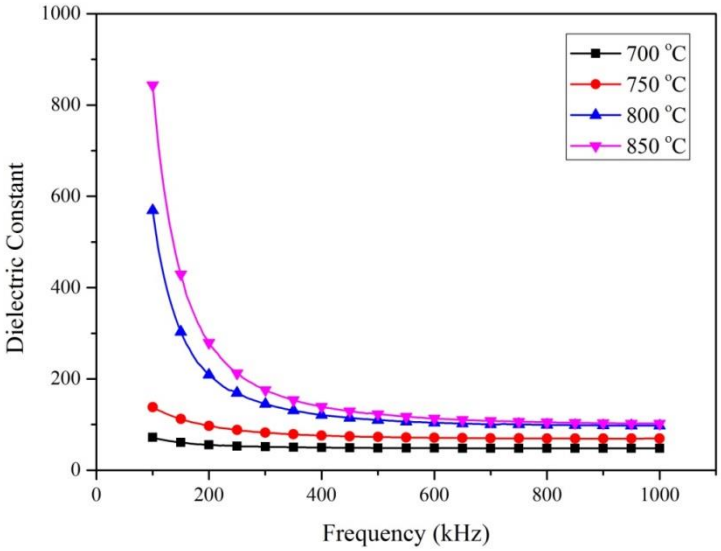

Figure 4.32 Dielectric constant-Frequency curves of BTS-BCT thin films sintered at different temperatures

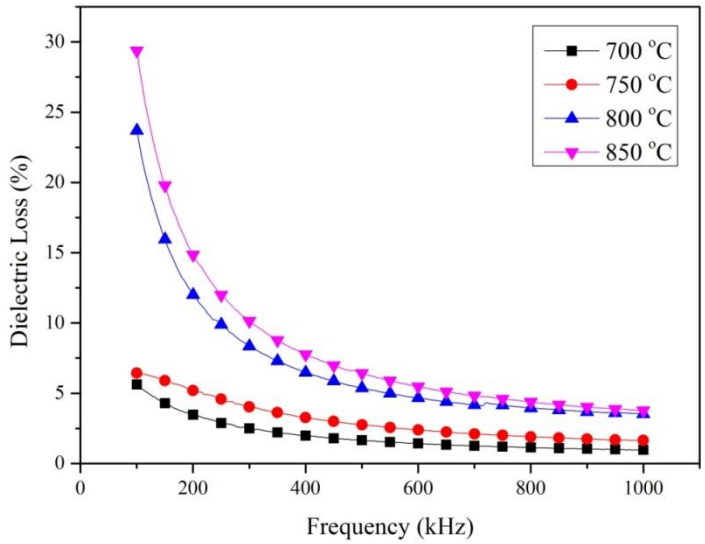

Figure 4.33 Dielectric loss-Frequency curves of BTS-BCT thin films sintered at different temperatures

4.6. Ferroelectric Properties of BTS-BCT Thin Films

In order to determine optimum sintering temperature for BTS-BCT thin films, ferroelectric properties of the films were studied carefully. Ferroelectric hysteresis

loops which illustrate the polarizations induced by electric field were examined. Ferroelectric properties of the thin films with four different sintering temperatures (700°C, 750°C, 800°C, and 850°C) were measured. The films were kept in sintering temperatures for 1 h and had thickness of 500 nm. In Table 4.3, between 1 to 10V applied electric field range, the remnant polarization and coercive field values of the BTS-BCT thin films sintered at different temperatures were listed. The highest voltage limit for BTS-BCT thin films with 500 nm is around 10V. In any voltage higher than 10V, dielectric breakdown occurs.

Table 4.3 Ferroelectric properties of the samples

Sintering Temperature (°C)	Remanent polarization (P_r) ($\mu C/cm^2$)				Coercive Field (E_c) (kV/cm)			
	1 V	3 V	5 V	10 V	1 V	3 V	5 V	10 V
700	0.06	0.19	0.35	0.90	2.6	8.1	14,3	34,5
750	0.17	0.49	0.90	1.59	3.1	10.0	17.4	32.8
800	0.28	0.93	1.87	3.10	4.5	14.6	27.7	43.3
850	0.29	0.92	1.73	4.11	4.2	14.5	24.3	57.8

Both of the hysteresis loops for samples sintered at 700°C and 750°C have relatively low remanent polarization and coercive field values. This is mainly caused by lower sintering temperatures. In Figure 4.2 which illustrates TG graph, it can be seen clearly that 783°C is a critical temperature where most of crystallization occurs. So because these samples were sintered below 783°C, the amount of crystallites which should give rise to polarization density may be limited. Figure 4.34 and Figure 4.35 show the hysteresis loops of BTS-BCT thin films sintered at 700°C and 750°C respectively. In Figure 4.34, the characteristics of the hysteresis loop which belongs to 700°C sintered sample is more like a paraelectric film due to limited amount of polarization. When 10V is applied, this sample has remnant polarization of 0.90 $\mu C/cm^2$.

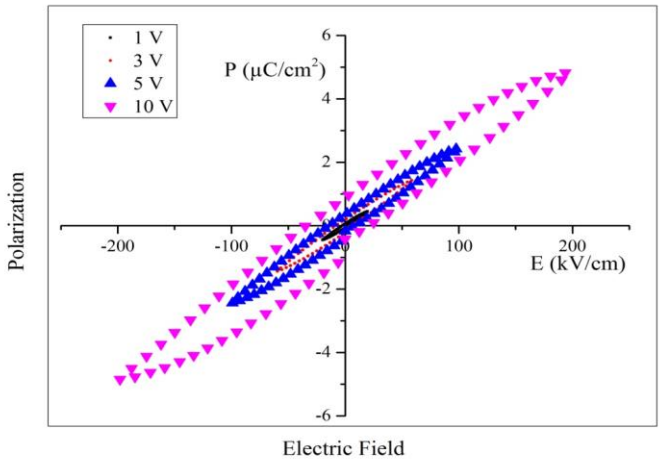

Figure 4.34 Hysteresis loops of BTS-BCT thin films sintered at 700 °C under different voltages

Nevertheless, sintering temperature gets closer to critical sintering temperature of 783°C, for the sample sintered at 750°C, the remanent polarization rises to 1.69 μC/cm^2 under 10V electric field applied. This sample has a slim but ideal hysteresis loop shape that reaches its maximum polarization of 7.80 μC/cm^2. The slim curve is mainly due to low polarization. However non-existence of pyrochlore enables the curve to have ideal curve that is at pre-saturation level which can be seen in Figure 4.35.

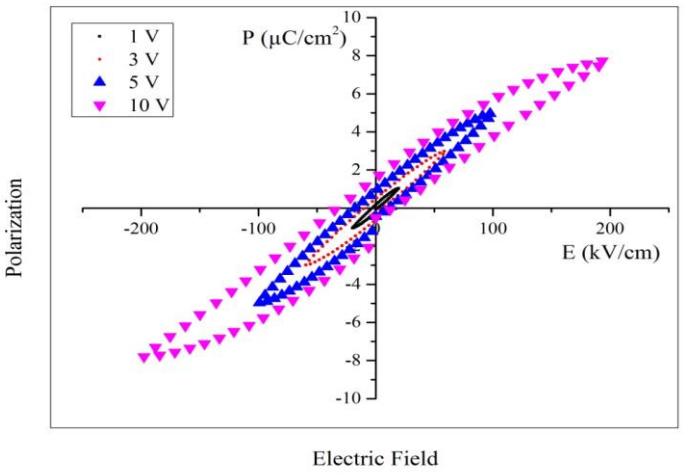

Figure 4.35 Hysteresis loops of BTS-BCT thin films sintered at 750°C under different voltages

As it can be seen clearly from Figure 4.36 and 4.37, BTS-BCT thin films sintered at 800°C and 850°C have higher polarization that can be understood from the fact that the hysteresis loops cover more area. The main factor to have these higher polarizations is due to have sintering temperatures higher than the critical sintering temperature of 783°C. When applied field is 10 V, the thin films sintered at 800°C and 850°C exhibit a remanent polarization of 3.10 μC/cm^2 and 4.11 μC/cm^2, and coercive field of 43.3kV/cm and 57.8 kV/cm, respectively. The sample sintered at 850°C is partially saturated.

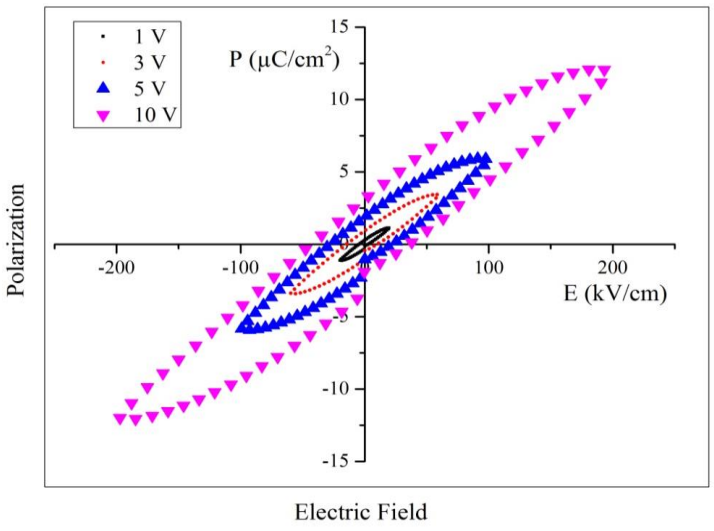

Figure 4.36 Hysteresis loops of BTS-BCT thin films sintered at 800°C under voltages

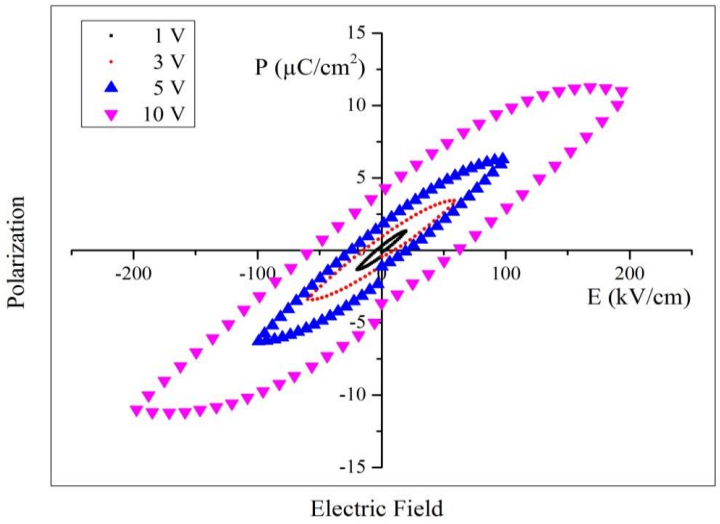

Figure 4.37 Hysteresis loops of BTS-BCT thin films sintered at 850°C under different voltages

For better understanding the ferroelectric behavior of BTS-BCT thin films, the comparison of the thin films sintered at different temperatures can be seen in Figures 4.38 and 4.39. In both of the figures, the thin films sintered at 800°C and 850°C have similar curves which indicate their polarization slightly increases with sintering temperature. On the other hand when these thin films are compared with films sintered at 700°C and 750°C, the induced remnant and maximum polarization significantly increases with annealing temperature. Furthermore, it can be clearly seen that as the sintering temperature increase the hysteresis loops shift toward vertical line and have larger areas. The remanent polarization and coercive field generally increase with sintering temperature except some exceptions. The sample sintered at 850°C has higher values but for 5V, the sample sintered at 800°C has slightly higher remnant polarization of 1.87μC/cm^2 and coercive field of 27.7 kV/cm when compared with the sample sintered at 850°C with remanent polarization of 1.73 μC/cm^2 and coercive field of 24.3 kV/cm. This situation can be caused by threshold of voltage that should be applied to thin films in order to promote domain rotation. In the situation where a higher voltage than 5V, 10V is applied, then sample sintered at 850°C has higher remnant polarization and coercive field values. Additionally, it should be noted that for BTS-BCT thin films, polarization increases more with higher sintering temperature when compared with coercive field. It should

be underlined that only the thin film sintered at 850°C is partially saturated, other films are not [98].

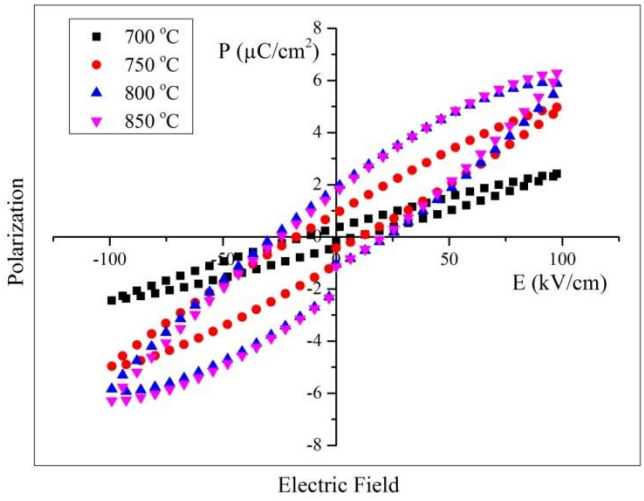

Figure 4.38 Hysteresis loops of BTS-BCT thin films sintered at different temperatures - 5 V applied

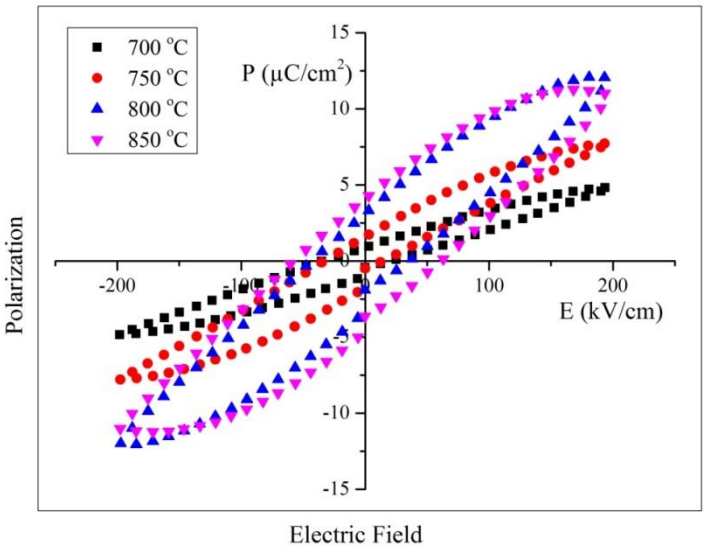

Figure 4.39 Hysteresis loops of BTS-BCT thin films sintered at different temperatures – 10 V applied

In Table 4.4 the comparison of $Ba(Ti_{0.88}Sn_{0.12})O_3-0.3(Ba_{0.7}Ca_{0.3})TiO_3$ thin films with other materials can be seen. When compared with lead free alternatives, PZT thin films holds superior electrical properties without any doubt. On the other hand, KNN and BNT based thin films have a breakthrough that results in piezolectric and dielectric values that reach nearly half values of PZT thin films. This breakthrough is not valid for BT thin films. Even though BT based materials in bulk form have superior ferroelectric, piezoelectric, dielectric properties, in thin film they can not exhibit similar behavior so that up to now no proper composition have been found to be an alternative for ferroelectric and piezoelectric applications. Generally this situation occurs due to densification problems, porous structure and randomly oriented-small sized grains.

Table 4.4 Electrical properties of the thin films in the literature

Composition	Piezoelectric displacement Coefficient d_{33} (pm/V)	Dielectric constant K (ϵ_r)	Dielectric loss (tan δ) (%)	Coercive field E_c (kV/cm)	Remnant polarization P_r ($\mu C/cm^2$)
[99] $Pb(Zr_{0.54}Ti_{0.46})O_3$	114	1084			17
[100] $Pb_{1.2}Zr_{0.52}Ti_{0.48}O_x$				39	45
[101] $Pb(Zr_{0.3}Ti_{0.7})O_3$		410	1.3	25.7	33
[63] $(K_{0.5}Na_{0.5})NbO_3$		452	1.7	100	12
[62] $K_{0.55}Na_{0.55}NbO_3$	46	540	5	70	7
[61] $(K_{0.44}Na_{0.52}Li_{0.04})(Nb_{0.84}NTa_{0.1}Sb_{0.06})O_3$	53			12	10
[61] Mn doped $(K_{0.44}Na_{0.52}Li_{0.04})(Nb_{0.84}NTa_{0.1}Sb_{0.06})O_3$	45			20	17
[68]$Bi_{0.5}(Na_{0.85}K_{0.15})_{0.5}TiO_3$	75	510			7
[67]La+Ce doped $(Bi_{0.5}Na_{0.5})_{0.94}Ba_{0.06}TiO_3$	31			74	29.5
[70]$Ba_{0.8}Sr_{0.2}TiO_3$		794		20	2.5
[102] $Ba_{0.9}Sr_{0.1}TiO_3$	19	780	0.6	40	13
[102] $BaTi_{0.98}Sn_{0.02}O_3$	5	820	2.6	40	3.5
[74] $Ba(Zr_{0.2}Ti_{0.8})O_3$ – 0.55$(Ba_{0.7}Ca_{0.3})$		350	3	33.7	2.8
[76]$Ba(Ti_{0.8}Zr_{0.2})O_3$-0.5$(Ba_{0.7}Ca_{0.3})TiO_3$		356	3.5	49.4	2.9
$Ba(Ti_{0.88}Sn_{0.12})O_3-0.3(Ba_{0.7}Ca_{0.3})TiO_3$		113	5.5	57.8	4.1

CHAPTER 5

SUMMARY, CONCLUSIONS AND FURTHER SUGGESTIONS

In this thesis study, as an alternative composition to lead based materials, $Ba(Ti_{0.88}Sn_{0.12})O_3$-$0.3(Ba_{0.7}Ca_{0.3})TiO_3$ thin films were fabricated by chemical solution deposition method. This composition was selected due to its location near morphotrophic phase boundary that exhibit large piezoelectric response as a bulk material. For the first time this composition has been fabricated in form of thin film. In this study, the microstructural and electrical properties of BTS-BCT thin films regarding the sintering temperature were characterized.

The fabrication of the BTS-BCT thin films began by preparing stable, stock solutions of 20ml. The molarity of the solutions was kept low in order to have many layers of coating that provides oriented growth of grains. Acetic acid and 2-methoxyethanol were proper solvents to dissolve the precursors without any precipitation problem. The viscosity measurement showed that the solution was Newtonian which means that the viscosity of the solution does not change much with shear rate, the solution is homogeneous and uniform.

Due to low thermal expansion coefficient of substrate, especially very low thermal expansion coefficient of top electrode of Pt and low mismatch between the lattice parameters of substrate and BTS-BCT thin films, the (111)-Pt/Ti/SiO_2/Si-(100) substrates was decided as the proper substrate. The thicknesses of the thin films coated on these substrates were determined as 500 nm due to two main reasons. The thinner films undergo dielectric breakdown while the thicker films form cracks due to high stress on the surface of the film. 500 nm film thicknesses were obtained through thirteen layers of spin coating with 2250 rpm for 30 s.

Thermal analysis from room temperature to 1000°C was conducted in order to determine critical changes in the material weight and heat exchange which helps to understand what steps are taken in which temperatures in heat treatment process. The main critical crystallization peak was determined as 783°C. According to results, the drying and firing temperatures for the thin films were decided as 200°C and 500°C respectively.

X-ray diffraction analysis was done in order to see how the microstructure is affected by the sintering temperature to BTS-BCT thin films. The diffractograms indicated that pure perovskite phase was obtained in the samples sintered at 700°C and 750°C. Because pure perovskite phase was obtained, the crystallization pattern of $BaTiO_3$ perovskite structure was obtained without intermediate phases. Beyond the critical sintering temperature, at 800°C and 850°C the material is more crystallized while a secondary phase, pyrochlore forms. At these temperatures the most desired peak of tetragonal structure which shows the oriented growth of grains with favorable polarization direction, the sharp peak of (111) perovskite can be observed.

SEM study revealed the surface morphology and film thicknesses of BTS-BCT thin films. The surface of the thin films was crack-free and relatively smooth except some contaminations from the air that can be observed in higher magnifications. In higher magnifications small grains ranging from 20 nm can be seen. The films have porous structure at 700°C. As temperature increases to 750°C, the grains form agglomerate like structures. At 800°C and 850°C, the material has a structure that is coexistence of agglomerate like large grain structure together with small grains. The grains are randomly oriented. Most likely, the (111) oriented grains are formed at the interface between the thin film and the top (111) Pt layer of the substrate but the dominant mechanism is the homogeneous nucleation of the grains at numerous nucleation sites within the thin film, as a result of morphological and structural analyses.

The control on the growth mechanism of the grains is very important for electrical properties. Promoting heterogeneous nucleation which results in columnar, oriented, large grains can be achieved by thinner films. So in this study, a relatively dilute solution and high spin coating speed was used in order to have thin layer thickness.

Even though this study had another aim to have highly oriented (111) columnar structure by fabricating the thin films by using very thin multiple layers (around 30-50nm thickness for one layer), the highly oriented columnar structure has not been achieved. This may be caused by formation of pyrochlore at the critical sintering temperatures. Additionally, a more dilute solution could be used to have thinner layers in each coating but fabricating 500 nm thin films with dilute solution of 0.1 M needs around 50 multiple layers which has its own problems, such as crack formation, very long fabrication period and higher contamination risk.

As a result of these studies, the dielectric property of BTS-BCT was measured between 100 kHz-1000 kHz. The results showed that at lower frequencies the material had higher dielectric properties, but important variation occurs with change in frequency except the thin film sintered at 700°C. So in those frequencies where dielectric constant changes much the material can not be used due to instability. But at 400 kHz and higher frequencies, the dielectric properties of the material are stable. The optimum result belongs to the sample sintered at 850°C with a permittivity and low loss tangent of 113.4 and 5.46 %, respectively, at 600 kHz.

Furthermore, BTS-BCT thin films were examined by ferroelectric hysteresis loops to understand the relation between the ferroelectric property and the sintering temperature. At optimum sintering temperature of 850°C, under electric field of 10 V the remnant polarization and coercive field values were found out as 4.11 $\mu C/cm^2$ and 57.8 kV/cm, respectively. Only the thin film sintered at 850°C had partially saturated hysteresis loop while others did not. The fact that the sample had partial saturation instead of having full saturation should be mostly caused by pyrochlore formation. There is another probability that the films should be sintered at higher temperatures than 850°C but it is not possible because the substrates have upper usage temperature limit of 850°C.

For enhancement of BTS-BCT thin films, the following suggestions can be suggested. Firstly, the elimination of pyrochlore can be achieved by Rapid Thermal Annealing. This method has short annealing time that reduces time but the temperature is enough to obtain desired physical or chemical processes are

completed. By this annealing method, undesired processes such as dopant diffusion, interface reactions, decomposition, or evaporation etc. can be suppressed or minimized so that denser microstructure can be obtained [103]. Additionally, using alcohol based Ba^{2+}, Ca^{2+} metal alkoxides instead of metal acetates to decrease sintering temperatures may contribute to fabrication of BTS-BCT films in order to eliminate pyrochlore formation and also for better morphologies with less roughness [76].

Next, the Curie temperatures of BTS-BCT compositions are low, close to room temperature (48°C). Smaller grain sizes even decrease the transition temperature of $BaTiO_3$ [104]. Combining BCTS composition with other alternatives such as BNT decreases depolarization temperature T_D significantly, even 10% BCTS content decreases T_D to 50°C [15]. There seems only one way to increase the transition temperature dramatically, an application of strain engineering. Biaxial compressive strain was applied to promote the ferroelectric properties of $BaTiO_3$ thin films. This strain, imposed by coherent epitaxy may provide higher temperature of ferroelectric transition nearly 500°C [105]. Additionally these films exhibited remnant polarization 250% higher than bulk $BaTiO_3$.

Another possible approach to promote electrical properties is to use solutions with low molarity for the coating. When these solutions with low molarity are used in together with pyrolysis step of each individual layer, heterogeneous, epitaxial growth and suppression of nucleation within the bulk of the film can be emphasized in perovskite grains such as BT [79].Lastly, adding seed layer may promote electrical properties [72].

To conclude, the dielectric and ferroelectric properties of BTS-BCT thin films were assessed with regard the morphological and microstructural results, hence sintering temperature of 850°C is chosen as optimum temperature for the fabrication of lead-free BTS-BCT thin films.

REFERENCES

[1] A. Safari, R. K. Panda, and V. F. Janas, "Ferroelectricity: Materials, Characteristics and Applications", Advanced Ceramic Materials: Key Engineering Materials, Vols. 122-124, Edited by M. Mostaghasi, Trans Tech Publications, pp. 35-71, (1996).

[2] Dubois MA, Muralt P. Measurement of the effective transverse piezoelectric coefficient of AlN and $Pb(Zr_x,Ti_{1-x})O3$ thin films. Sensors Actuators 1999;77:106–12.

[3] Hsu Yi-Chu, Wu Chia-Che, Lee Cheng-Chun, Cao GZ, Shen IY. Demonstration and characterization of PZT thin-film sensors and actuators for meso- and micro-structures. Sensors Actuators 2004;A116:369–77.

[4] Safari, A., & Abazari, M. (2010). Lead-Free Piezoelectric Ceramics and Thin Films, *57*(10).

[5] Panda, P. K. (2009). Review : environmental friendly lead-free piezoelectric materials. *Journal of Materials Science (full set)*, 5049-5062. doi:10.1007/s10853-009-3643-0

[6] Muralt, P. (2000). Ferroelectric thin films for micro-sensors and actuators : a. *In Situ*, *10*, 136-146.

[7] Shen, I. Y. S., Cao, G. Z., Wu, C.-che, & Lee, C.-chun. (2006). PZT Thin-Film Meso- and Micro Devices, 15-34. doi:10.1080/00150190600946062

[8] "DIRECTIVE 2011/65/EU: Restriction of the use of certain hazardous substances in electrical and electronic equipment (RoHS)," *Off. J. Eur. Union*, vol. 54, L174, pp. 88-104, 2011.

[9] DIRECTIVE 2012/19/EU: waste electrical and electronic equipment (WEEE). Off J Eur Union , vol 55 ,L197, pp. 38-71, 2012.

[10] T.C. Resmi Gazete, 26891, 2008

[11] Shrout, T. R., & Zhang, S. J. (2007). Lead-free piezoelectric ceramics : Alternatives for PZT ? *Journal of Electroceramics*, (September 2006), 111-124.

[12] Smeltere I., "Lead-Free Ferroelectric Ceramics Based on Alkali" , Summary of the Doctoral Thesis, RIGA Technical University, 2013

[13] Pal, V., Dwivedi, R. K., & Thakur, O. P. (2013). Effect of Processing on Synthesis and Dielectric Behavior of Bismuth Sodium Titanate Ceramics. *Ceramics*, *2013*.

[14] Xue, D., Zhou, Y., Bao, H., Gao, J., Zhou, C., & Ren, X. Large piezoelectric effect in Pb-free Ba(Ti ,Sn)O_3 -x (Ba,Ca)TiO_3 ceramics, *122901*(2011), 8-11.

[15] Bao, H., Zhou, C., Xue, D., & Gao, J. (n.d.). A modified lead-free piezoelectric BTS– x BCT system with higher T C, *465401*. doi:10.1088/0022-3727/43/46/465401

[16] Ma, S., Ji, W., Li, W., Gong, S., & Li, G. (2014). Enhanced piezoelectricity in broad composition range and the temperature dependence research. *Physica B: Physics of Condensed Matter*, *433*, 43-47. Elsevier.

[17] Chen M., Xu, Chu R., Liu Y., Shao L., Li W., ,Gong S., Li G., Polymorphic phase transition and enhanced piezoelectric properties of $Ba_{0.90}Ca_{0.10}Ti_{1-x}Sn_xO_3$ lead-free ceramics, Materials Letters 97 (2013) 86-89

[18] Li W., Xu Z, Chu R., Fu P., Zang G., Enhanced ferroelectric properties in $(Ba_{1-x}Ca_x)(Ti_{0.94}Sn_{0.06})O_3$, Journal of the European Ceramic Society, 32 (2012) 517-520

[19] Liu, W., & Ren, X. (2009). Large Piezoelectric Effect in Pb-Free Ceramics, *257602*(December), 1-4. doi:10.1103/PhysRevLett.103.257602

[20] Damjanovic, D., Klein, N., & Li, J. I. N. (2010). What can be expected from Lead-free Piezoelectric Materials?Why is PZT a Good Piezoelectric Material? *Materials Letters*, *3*(1), 5-13.

[21] W. D. Callister, J., Materials Science and Engineering An Introduction. New York: Wiley, 2009, 8th edition.

[22] MIT Study Guide, Chapter 5, Capacitance and Dielectrics

[23] http://www.ami.ac.uk/courses/topics/0184_dp/ [Last accessed on 29.01.2015]

[24] C. Cohn, Agere Systems, Electronic materials and Processes Handbook

[25] R.E. Hummel, Electronic Properties of Materials, n.d.Electronic Materials and Processes Handbok 3rd Edition

[26] inSiDE • Vol. 9 No. 1 • Spring 2011 Mariana Lezaic, Research Centre Jülich Cohn, C. (n.d.). Development and Fabrication of IC Chips. *Library*.

[27] Damjanovic, D. (1998). Ferroelectric , dielectric and piezoelectric properties of ferroelectric thin films and ceramics, *61*, 1267-1324.

[28] Cambridge University, Teaching and Learning Packages, Ferroelectrics, U.K., December 2006

[29] M. Dawber, K.M. Rabe, J.F. Scott, Physics of thin-film ferroelectric oxides, Reviews of modern physics, APS, 2005

[30] Dielectric Materials and Applications, Edited by Arthur R. Von Hippel, pp. 19, 1954.

[31] Vatansever, D., Siores, E., & Shah, T. (2012). Alternative Resources for Renewable Energy : Piezoelectric and Photovoltaic Smart Structures. *Perspective*.

[32] Yuhuan Xu . (1991). *Ferroelectric materials and their applications*. Netherlands: North-Holland.

[33] *The physics of ferroelectric memories*, Auciello O, Scott JF, Ramesh R., Physics Today 51, p22, July 1998

[34] Alexe, M. (2005). I. Ferroelectric materials for piezoelectric, pyroelectric, and memory applications

[35] Setter, N., Damjanovic, D., Eng, L., Fox, G., Gevorgian, S., Hong, S., Streiffer, S. (2006). Ferroelectric thin films: Review of materials, properties, and applications. *Journal of Applied Physics*, *100*(5), 051606.

[36] J.F. Scott and C Araujo, "Ferroelectric Memories", Science, Vol. 246, 1400-1405, 1989

[37] S.O. Kasap, Principles of electronic materials and devices third edition,2005

[38] S. D. Hutagalung, School of materials & Mineral Resourses Engineering, EBB 443

[39] Cambridge University, Teaching and Learning Packages, Piezoelectrics, U.K., November 2007

[40]http://www.morganelectroceramics.com/resources/piezo-ceramic-tutorials/typical-properties/ [Last accessed on 29.01.2015]

[41] A.O.M. Corbino, C. Nazionale, Chapter 4 PIEZOELECTRIC THIN FILMS : PROCESSING AND PROPERTIES , 2002.

[42] Unlimited, F., Required, P., & Block, S. (n.d.). Non-Volatile Ferroelectric Random Access Memory (FRAM).

[43] Y. Saito, H. Takao, in 12th US–Japan Seminar on Dielectric and Piezoelectric Ceramics, ed. By C. Wu, H. Kishi, C. Randall, P. Pinceloup, H. Funakubo, (Maryland, 2005), pp. 103–107

[44] Y. Saito, H. Takao, T. Tani, T. Nonoyama, K. Takatori, T. Homma, T. Nagaya,

M. Nakamura, Lead-free piezoceramics, Nature 432 (7013) (2004).

[45] Safari, A., & Abazari, M. (2010). Lead-free piezoelectric ceramics and thin films. *IEEE Transactions on Ultrasonics, Ferroelectrics, and Frequency Control*, *57*(10), 2165–76. doi:10.1109/TUFFC.2010.1674

[46] Y . Dai, X. Zhang, and G. Zhou, "Phase transitional behavior in $K_{0.5}Na_{0.5}NbO_3$–$LiTaO_3$ ceramics," *Appl. Phys. Lett.*, vol. 90, no. 26, art. no. 262903, 2007.

[47] Guo, K.-I. Kakimoto, and H. Ohsato, "$(Na_{0.5}K_{0.5})NbO_3$–$LiTaO_3$ lead-free piezoelectric ceramics," *Mater. Lett.*, vol. 59, no. 2–3, pp. 241–244, 2005.

[48] Zhengfa, Li, Li Yongxiang, and Zhai Jiwei. "Grain growth and piezoelectric property of KNN-based lead-free ceramics." *Current Applied Physics* 11.3 (2011): S2-S13.

[49] T. Takenaka, K. Maruyama, and K. Sakata, "$(Bi_{1/2}Na_{1/2})TiO_3$- $BaTiO_3$ system for lead-free piezoelectric ceramics," *Jpn. J. Appl. Phys.*, pt. 1, vol. 30, no. 9B, pp. 2236–2239, 1991.

[50] D. Lin, D. Xiao, J. Zhu, and P. Yu, "Piezoelectric and ferroelectric properties of $[Bi_{0.5}(Na_{1-x-y}K_xLi_y)_{0.5}]TiO_3$ lead-free piezoelectric ceramics," *Appl. Phys. Lett.*, vol. 88, no. 6, art. no. 062901 2006.

[51] Hiruma, H. Nagata, and T. Takenaka, "Phase transition temperatures and piezoelectric properties of $(Bi_{1/2}Na_{1/2})TiO_3$–$(Bi_{1/2}K_{1/2})TiO_3$–$BaTiO_3$ lead-free piezoelectric ceramics," *Jpn. J. Appl. Phys.*, pt. 1, vol. 45, no. 9B, pp. 7409–7412, 2006.

[52] Thurnauer H. ,The Rochester Engineer, Vol. 21, 74-75, 1947.

[53] O. P. Thakur, C. Prakash, and A. R. James, Journal of Alloys and Compounds, Vol. 470, 548-551, 2009.

[54] X. S. Wang, H. Yamada, and C. N. Xu, Applied Physics Letters, Vol. 86, 022905, 2005

[55] S. J. Zhang, E. F. Alberta, R. E. Eitel, C. A. Randall, and T. R. Shrout, IEEE Trans. Ultrason. Ferroelectr. Freq. Control 52, 2131 (2005)

[56] M. Ahart et al., Nature (London), Vol. 451, 545 2008.

[57] H. X. Fu and R. E. Cohen, Nature (London), Vol. 403, 281, 2000.

[58] G. A. Rossetti, A. G. Khachaturyan, G. Akçay, and Y. Ni, Journal of Applied Physics, Vol. 103, 114113, 2008.

[59] M. Abazari, E. K. Akdogan, and A. Safari, "Effect of manganese doping on remnant polarization and leakage current in $(K_{0.44},Na_{0.52},Li_{0.04})(Nb_{0.84},Ta_{0.10},Sb_{0.06})O_3$ epitaxial thin films on $SrTiO_3$," *Appl. Phys. Lett.*, vol. 92, no. 21, art. no. 212903, 2008.

[60] M. Abazari, T. Choi, S. W. Cheong, and A. Safari, "Nanoscale characterization and local piezoelectric properties of lead-free KNN-LT-LS thin films," *J. Phys. D Appl. Phys.*, vol. 43, no. 2, art. no. 025405, 2010.

[61] C . W. Ahn, E. D. Jeong, S. Y. Lee, H. J. Lee, S. H. Kang, and I. W. Kim, "Enhanced ferroelectric properties of $LiNbO_3$ substituted N $a_{0.5}K_{0.5}NbO_3$ lead-free thin films grown by chemical solution deposition," *Appl. Phys. Lett.*, vol. 93, no. 21, art. no. 212905, 2008.

[62] K, M., Akashima, Y. N., Akamoto, W. S., Aiwa, H. M., et al. (n.d.). Lead-Free Piezoelectric (K,Na)NbO_3 Thin Films Derived from Metal Alkoxide Precursors JJAP Express Letter. *Japanese Journal of Applied Physics*, *311*, 12-15.

[63] Wu, J., & Wang, J. (2009). Phase transitions and electrical behavior of lead-free $(K_{0.50}Na_{0.50})NbO_3$ thin film. *Journal of Applied Physics*, *106*(6), 066101.

[64] Harada, S., & Muralt, P. (n.d.). Pulsed laser deposition of KNN-based ferroelectric thin films on platinised Si substrates. *Materials Science, 012004*.

[65] X.-G. Tang, J. Wang, X.-X. Wang, and H. L.-W. Chan, "Preparation and electrical properties of highly (111)-oriented ($Na_{0.5}Bi_{0.5}$) TiO_3 thin films by a sol-gel process," *Chem. Mater.*, vol. 16, no. 25, pp. 5293–5296, 2004.

[66] D. Y. Wang, D. M. Lin, K. S. Wong, K. W. Kwok, J. Y. Dai, and H. L. W. Chan, "$BaTiO_3$ thin films by pulsed laser deposition Piezoresponse and ferroelectric properties of lead-free $(Bi_{0.5}Na_{0.5})_{0.94}Ba_{0.06}TiO_3$" vol. 5, no. 2008, pp. 2006-2009, 2013.

[67] Wang et. al."Enhanced ferroelectric and piezoelectric properties in doped lead-free," *Applied Physics*, vol. 97, no. 21, pp. 5-8, 2010.

[68] Wang N. K. Tio et al., "Large piezoresponse of lead-free $Bi_{0.5}(Na_{0.85}K0.15)0.5TiO_3$ thin film," *Current Applied Physics*, vol. 12, no. 3, pp. 903-907, 2012.

[69] M.-C. Wang, F.-Y. Hsiao, C.-S. Hsi, and N.-C. Wu, "Crystal structure and ferroelectricity of nanocrystalline barium titanate thin films," *J. Cryst. Growth*, vol. 246, no. 1–2, pp. 78–84, Dec. 2002.

[70] F. M. Pontes, E. Longo, E. R. Leite, and J. A. Varela, "Study of the dielectric and ferroelectric properties of chemically processed $Ba_x Sr_{1-x} TiO_3$ thin films," pp. 91–98, 2001.

[71] S. H. Xiao, W. F. Jiang, K. Luo, J. H. Xia, and L. Zhang, "Structure and ferroelectric properties of barium titanate films synthesized by sol–gel method," *Mater. Chem. Phys.*, vol. 127, no. 3, pp. 420–425, Jun. 2011.

[72] L. Gao, J. Zhai, S. Song, and X. Yao, "Enhanced Dielectric Properties of Ba(Sn $_{0.15}$ Ti $_{0.85}$)O_3 Thin Films Grown on Pt/Ti/SiO_2/Si Substrates," *Ferroelectrics*, vol. 405, no. 1, pp. 191–197, Oct. 2010.

[73] Z. Jiwei, S. Bo, Y. Xi, and Z. Liangying, "Dielectric and ferroelectric properties of $Ba(Sn_{0.15}Ti_{0.85})O_3$ thin films grown by a sol–gel process," *Mater. Res. Bull.*, vol. 39, no. 11, pp. 1599–1606, Sep. 2004.

[74] Y. Lin, G. Wu, N. Qin, and D. Bao, "Structure, dielectric, ferroelectric, and optical properties of $(1-x)Ba(Zr_{0.2}Ti_{0.8})O_3-x(Ba_{0.7}Ca_{0.3})TiO_3$ thin films prepared by sol–gel method," *Thin Solid Films*, vol. 520, no. 7, pp. 2800–2804, Jan. 2012.

[75] A. Piorra, A. Petraru, H. Kohlstedt, M. Wuttig, and E. Quandt, Journal of Applied Physics, Vol. 109, 104101, 2011.

[76] B. Çeltikçi, M. Özenbaş, Preparation of BZT-BCT Thin Films by Chemical Solution Deposition and Their Characterization , M.S. Thesis (Supervisor: Prof. Dr. Macit Özenbaş), Middle East Technical University, Ankara-Turkey, 1996.

[77] Novel Materials from Solgel Chemistry. (2005), (May), 24–26.

[78] A. C. Pierre, Introduction to Sol-Gel Processing. Boston : Kluwer Academic Publishers,1998.

[79] R. W. Schwartz, T. Schneller, R. Waser, Comptes Rendus Chimie, 433-461, 2004.

[80] D. E. Bornside, C. W. Macosco and L. E. Scriven, Journal of Imaging Technology, Vol. 13, 122-129, 1987.

[81] E. İzgi, Characterization of Superconducting Bi-Sr-Ca-Cu-O System Prepared by Sol-Gel Processing. M.S. Thesis (Supervisor: Prof. Dr. Macit Özenbaş), Middle East Technical University, Ankara-Turkey, 1996.

[82] I.M. Reaney, K. Brooks, R. Klissurka, C. Pawlaczyk, N. Setter J. Am. Ceram. Soc., Vol. 77, 1209, 1994.

[83] E.M. Griswold, L. Weaver, M. Sayer, J.D. Calder J. Mater. Res., Vol. 10, 3149, 1995.

[84] A.P. Wilkinson, J.S. Speck, A.K. Cheetham, S. Nataraan, J.M. Thomas Chem. Mater., Vol. 6 , 750, 1994.

[85] Mathematica's Element Data function, Wolfram Research Inc.

[86] J. Yan-ping, T. Xin-gui, and L. I. U. Qiu-xiang, "XPS study of BZT thin film deposited on Pt/Ti/SiO_2/Si substrate by pulsed laser deposition," *Thin Films*, no. 100, pp. 2-5, 2007.

[87] B.M. Vehkamäki, T. Hatanpää, M. Ritala, M. Leskelä, S. Väyrynen, E. Rauhala, Atomic Layer Deposition of $BaTiO_3$ Thin Films – Effect of Barium Hydroxide Formation, (2007) 239–246. doi:10.1002/cvde.200606538.

[88] M. H. M. Zai, A. Akiba, H. Goto, M. Matsumoto, and E. M. Yeatman, "Highly (111) oriented lead zirconate titanate thin films deposited using a non-polymeric route," *Thin Solid Films*, pp. 97-101, 2001.

[89] Hoffmann S. Waser R., Control of the Morphology of CSD-prepared (Ba,Sr)TiO3 Thin Films, Journal of European Ceramic Society, 19, 1339-1343, 1999

[90] Schwartz R. W., Chemical Deposition of Perovskite Thin Films, Chem. Mater. 1997, 9, 2325-2340

[91] C. Kügeler et al., Inst. of Solid State Res. & Jara-Fundamentals for Future Inf. Technol., Jülich, Germany, 2006

[92] N. Horchidan, A.C. Ianculescu, C.A. Vasilescu, M. Deluca, V. Musteata, H. Ursic, et al., Multiscale study of ferroelectric–relaxor crossover in $BaSn_xTi_{1-x}O_3$ ceramics, J. Eur. Ceram. Soc. 34 (2014) 3661–3674.

[93] Bernard Jaffe, Piezoelectric Ceramics, London, New York, Academic Press, 1971.

[94] Cambridge University, Teaching and Learning Packages, Dielectrics, April 2009

[95] M. Nayak, S. Y. Lee and T. Y. Tseng, Electrical and Dielectric Properties of $(Ba_{0.5}Sr_{0.5})TiO_3$ Thin Films Prepared by a Hydroxide-Alkoxide Precursor- Based Sol-Gel Method. Materials Chemistry and Physics, 2002, 77, p. 34

[96] M.R. Baklanov, K. Maex, Porous low dielectric constant materials for microelectronics., Philos. Trans. A. Math. Phys. Eng. Sci. 364 (2006) 201–215.

[97] Zhu X H, Zheng D N, Zeng H, Peng W, Zhu J G, Yuan X W, Yong L P, Miao J, Li J, Tian H Y, Xu X P. "Effects of growth temperature and film thickness on the electrical properties of $Ba_{0.7}Sr_{0.3}TiO_3$ thin films grown on platinized silicon substrates by pulsed laser deposition" [J].Thin Solid Films, 2006, 496: 376−382.

[98] Y. Gong, X. Zheng, L. Gong, Y. Ma, D. Zhang, S. Dai, et al., "Effects of annealing temperature on microstructure and ferroelectric properties of $Bi_{0.5}(Na_{0.85}K_{0.15})_{0.5}TiO_3$ thin films", Trans. Nonferrous Met. Soc. China. 20 (2010) 1906–1910.

[99] Sama N., Herdier R., Jenkins D., Soyer C, Detalle M., "On the influence of the top and bottom electrodes – a comparative study between Pt and LNO electrodes for PZT thin films", Journal of Crystal Growth, 2008; 310:3299-302

[100] Li X., Tanaka T., Suzuki Y., "Preferred orientation and ferroelectric properties of lead zirconate titanate thin films", Thin Solid Films, 375 (2000) 91-94

[101] Sun LL., Tan OK., Liu WG., Chen XF., Zhu W., Comparison study on sol-gel $Pb(Zr_{0.3}Ti_{0.7})O_3$ and $Pb(Zr_{0.3}Ti_{0.7})O_3$ /$PbTiO_3$ mutilayer thin films for pyroelectric infrared detectors, Microelectron Eng 2003; 66: 738-44

[102] Fasquelle D., Mascot M., Carru J.C., "On the research of lead-free material challengers for PZT replacement", Solid-State Electronics, 75 (2012) 6-12

[103] Umut Adem, "Preparatiom of $Ba_xSr_{1-x}TiO_3$ Thin Films by Chemical Solution Deposition and Their Characterization", M.S. Thesis, Middle East Technical University, Ankara Turkey, (2003)

[104] C. A. Randall, D. E. McCauley and D. P. Cann , Finite Size Effects in a $BaTiO_3$ Ferroelectric Glass Ceramic, Ferroelectrics, Vols. 206-207, pp. 325-335,1998

[105] Choi, K. J., M. Biegalski, Y. L. Li, and A. Sharan, enhancement of ferroelectricity in strained $BaTiO_3$ films. Science 5 November 2004: Vol. 306 no. 5698 pp. 1005-1009